The reactivity of methanimine radical cation (H2CNH.+) and its isomer aminomethylene (HCNH2.+) with C2H4

D. Sundelin, D. Ascenzi, V. Richardson, C. Alcaraz, M. Polásek, C. Romanzin, R. Thissen, P. Tosi, J. Žabka, W. Geppert

The reactivity of methanimine radical cation ($H_2CNH^{\bullet+}$) and its isomer aminomethylene ($HCNH_2^{\bullet+}$) with C_2H_4

D. Sundelin[a], D. Ascenzi[b], V. Richardson[b], C. Alcaraz[c,d], M. Polášek[e], C. Romanzin[c,d], R. Thissen[c,d], P. Tosi[b], J. Žabka[e] and W. Geppert[a *]

[a] Department of Physics, Stockholm University, Roslagstullsbacken 21, 10691 Stockholm, Sweden

[b] Department of Physics, University of Trento, Via Sommarive 14 – 38123 Italy

[c] Université Paris-Saclay, CNRS, Institut de Chimie Physique, UMR8000, 91405 Orsay, France

[d] Synchrotron SOLEIL, L'Orme des Merisiers, F-91192 Saint Aubin, Gif-sur-Yvette, France

[e] J. Heyrovsky Institute of Physical Chemistry of the Czech Academy of Sciences, Dolejškova 3, Prague 8, 18223 Czech Republic

* corresponding author: e-mail wgeppert@fysik.su.se phone: ++ 46 8 5537 8649

Keywords: interstellar medium; rate constant; ion-molecule reactions; astrochemistry molecular astrophysics; isomerism; Titan's atmosphere; protonated ketenimine

Graphical abstract

Abstract

Experimental and theoretical studies are presented on the reactivity of $H_2CNH^{\bullet+}$ (methanimine) and $HCNH_2^{\bullet+}$ (aminomethylene) with ethene (C_2H_4). Selective isomer generation is performed via dissociative photoionization of suitable neutral precursors and reactive cross sections and branching ratios are measured as a function of photon and collision energies. Differences between isomers' reactivity are discussed in light of *ab-initio* calculations on reaction mechanisms. The main products, for both isomers, are H-elimination, most likely occurring from covalently bound adducts (giving c-$CH_2CH_2CHNH^+$/$CH_2NHCHCH_2^+$) and $H^{\bullet}$ atom transfer to yield $H_2CNH_2^+$. The astrochemical implications of the results are briefly addressed.

1. Introduction

Ion-induced processes have long been regarded as playing a pivotal role in the synthesis of complex molecular species in the interstellar medium, as well as the atmospheres of planets and their satellites[1]. Increasingly complex ions have been detected using state-of-the-art terrestrial single-dish telescopes and interferometers, and with this increase in complexity the role of isomers becomes crucial. Isomers have different spectroscopic and chemical properties and, since isomerisation barriers for many species are too high to be overcome thermally under interstellar conditions, they have to be treated as different species with distinctive chemical reactivities in astrochemical models. The existence of

isomeric ions in the interstellar medium has long been known, and in the case of HCO^+ and HOC^+ their relative abundance ratio has been assessed[2] allowing conclusions to be drawn about the chemistry of their environments.

Whereas ionic isomers often possess different dipole moments and other spectroscopic properties, and so can be distinguished in radioastronomic observations[2], assessment of ion abundances in planetary and satellite atmospheres often relies on mass spectrometers, which cannot distinguish between isomers. As a result, their relative abundances often remain elusive in those environments. However, the novel Atacama Large Interferometer Array (ALMA) allows for the collection of column density information as a function of altitude for HCN and HNC[3]. The unprecedented resolution of ALMA will also permit the retrieval of data about the abundance and distribution of isomeric ions in different astronomic environments. In order to perform model calculations rationalising these abundances, it is important to assess the reactivity of ionic isomers with common interstellar and atmospheric molecules.

In recent years, studies have been undertaken using suitable precursor molecules to either purely or preferentially produce a single isomer [4]. VUV photoionisation has proven to be an especially versatile tool for selective production of isomers[5] while noble gas tagging has also been successfully employed to characterise isomeric ions and to determine their relative abundance after electron ionisation using different neutral precursors[6].

Titan is one of the most interesting objects in the solar system as it possesses a dense nitrogen-dominated atmosphere[7] similar to our own planet. The ion and neutral mass-spectrometer (INMS) onboard the Cassini spacecraft dicovered that Titan's atmosphere is one of the most complex in the solar system, containing large hydrocarbons and nitrogen-bearing compounds[8, 9]. This varied chemistry originates from the dissociation of its main components N_2 and CH_4 by either extreme ultraviolet (EUV) radiation[10] or magnetospheric electrons. The resultant ions and radicals can subsequently undergo ion-neutral and radical-neutral reactions leading to more complex compounds[11, 12]. Ion-neutral pathways involving unsaturated hydrocarbons (*e.g.* ethyne and ethene) in particular are frequently held responsible for the production of complex ions detected in Titan's atmosphere[12, 13]. Positive ions with masses up to 99 amu were detected by INMS at altitudes of 950 km above the surface and the presence of cations with higher masses (up to 350 amu) were observed with the Cassini plasma spectrometer ion beam sensor (CAPS-IBS)[14]. It is therefore important to investigate the production routes of these species and the reaction of nitrogen-containing ions with hydrocarbons could play a decisive role in that. However, many of these species are protonated nitriles which are comparatively unreactive and mostly destroyed by dissociative recombination in Titan's atmosphere[15]. Contrastingly, $H_2CNH^{\bullet+}$ and its isomer $HCNH_2^{\bullet+}$ are reactive radical cations and could act as a template for the formation of larger neutral molecules through chain elongation reactions with unsaturated and saturated hydrocarbons followed by dissociative recombination of the resulting cations.

Although the mass signal at *m/z* 29 recorded by INMS can largely be attributed to a mixture of $C_2H_5^+$ and $H^{13}CNH^+$ ions, model calculations predict a density of $HCNH_2^{\bullet+}$ and its isomers

amounting to 1.1 × 10^{-2} cm^{-3} in Titan's ionosphere[15]. These species may therefore play a role in the build-up of larger nitrogen-containing species which can then further react to form aerosols associated with Titan's orange-coloured haze. This paper presents a reactivity study of $H_2CNH^{\bullet+}$ and its isomer $HCNH_2^{\bullet+}$ with ethene using synchrotron radiation and suitable precusors to selectively generate the charged species.

2. Methodology

The experimental and theoretical methodologies used have already been decribed in detail in an accompanying paper to this Special Issue devoted to reactivity of the title ions with C_2H_4 [16] as well as in Ref. [17], so only the briefest of summaries is given here.

2.1 Experimental Set-Up

Experiments were performed using the CERISES apparatus[17,18], at the DESIRS beamline[19] of the SOLEIL synchrotron radiation facility. CERISES is a guided ion beam tandem mass spectrometer composed of two octopoles located between two quadrupole mass filters. $[H_3CN]^{\bullet+}$ isomers were produced by dissociative photoionization (in the photon energy range E_{phot} = 9.5-13.5 eV) of gaseous precursors (see **Section 2.3**) introduced into the ion source at roughly 10^{-6} mbar. Ethene was introduced into the reaction cell (surrounding the first octopole) at a dynamic pressure of 2.6 x10^{-7} bar, which guarantees operation close to a single collision regime, reduces secondary reactions and limits the parent ion attenuation to less than 10%. Collision energies in the lab depend on the ion charge and on the difference between the ion source and reaction cell potentials. The retarding potential method[20] was used to determine the point which corresponds to the maximum of the first derivate of the parent ion yield, which in turn defines the zero point of the kinetic energy. The parent beam FWHM is 400 mV, which corresponds to 0.196 eV in the centre-of-mass frame. By changing the potentials of the reaction cell and all subsequent elements up to 20V, the collision energy (E_{CM}) can be increased up to 9.82 eV in the centre-of-mass frame.

2.2 Theoretical Methodology

The reaction mechanisms for both isomers were studied using GAUSSIAN[21]. Intermediate structures were calculated at the MP2/6-31G*, MP2/6-311++G** and MP2/cc-pVTZ level and the identities of transition states and minima were checked by frequency calculations and zero-point energy corrections were applied to the resultant energies. IRC calculations were performed at the MP2/6-31G* level to ensure that the transition states connect the correct minima. The dissociation pathways were probed through relaxed potential energy surface scans along the dissociation coordinates of the corresponding minima. In some cases it was necessary to fix one or two angles and a dihedral angle including the dissociating bond to avoid the scan leading to another adduct. Single point energy calculations were carried out for all stationary points at the CCSD(T)/6-311++G**and CCSD(T)/cc-pVTZ levels with zero-point energy corrections taken from the MP2/6-

311++G** and MP2/cc-pVTZ levels, respectively. In both cases the geometries were optimised at the MP2/cc-pVTZ level. Full results are given in the **Supplementary Information - Part 1.**

2.3 Ions generation and checks on impurities

The generation of the two ions through dissociative photoionization of different neutral precursors is described elsewhere[16]. Due to lack of space, the reader is referred to such references and to the **Supplementary Information - Part 2** of this work for a detailed discussion of the potential impact of isobaric impurities ($C_2H_5^+$, $H^{13}CNH^+$ and $^{13}CCH_4^{\bullet+}$) on the reaction with C_2H_4. Only the main conclusions are reported here.

The $HCNH_2^{\bullet+}$ and $H_2CNH^{\bullet+}$ isomers are generated from dissociative photoionization of cyclopropylamine (*c*-$C_3H_5NH_2$) and azetidine (c-$CH_2CH_2CH_2NH$)[22, 23, 24] respectively. In both cases the experimental appearance energies of fragments at *m/z* 29 are 10.2±0.1 eV[16]. Theoretical calculations, control experiments performed by mass selecting parent ions at *m/z* 28 from both azetidine and cyclopropylamine and literature data on the reactivity of $C_2H_5^+$, $C_2H_4^+$ and $HCNH^+$ with C_2H_4 [25] allowed us to conclude that:

a) dissociative photoionization of cyclopropylamine at photon energies above ~12.4 eV leads to contamination from $C_2H_5^+$ which can react with C_2H_4 to give $C_3H_5^+$ (*m/z* 41). This contamination channel seems less relevant in the azetidine case.
b) although the production of $HCNH^+$ from dissociative photoionization of both precursors has similar appearance energies to $HCNH_2^{\bullet+}$/$H_2CNH^{\bullet+}$ [16], the reaction of $HCNH^+$ with C_2H_4 is endothermic and leads exclusively to the proton transfer product $C_2H_5^+$. We therefore expect any contamination from $H^{13}CNH^+$ in the reagent beam not to interfere with the results discussed in the following.
c) dissociative photoionization of azetidine at photon energies above ~11.3 eV leads to a small contamination from $C_2H_4^{\bullet+}$ which can react with C_2H_4 to give $C_3H_5^+$ (*m/z* 41) plus a minor amount of $C_4H_7^+$ (*m/z* 55). However, since the ratio of the photodissociation yields for *m/z* 28 and 29 at the explored photon energies is in the range 0.3-1.0, we expect a small contamination of $^{13}CCH_4^{\bullet+}$ in the reagent beam, which may be responsible of the small signal observed at *m/z* 41 but does not interfere with the results presented here.

3. Results and discussion: reactivity experiment

The reaction of both isomers yielded products at *m/z* 30, 42 and 56 with the reaction of $H_2CNH^{\bullet+}$ also showing a product at *m/z* 28 significant enough to be separated from the parent signal. This is not the case for the $HCNH_2^{\bullet+}$ for which only an upper limit of ~0.8 Å^2 for the cross section of *m/z* 28 product could be estimated from a mass spectrum taken at E_{CM}=0.13 eV and E_{phot}=11.48 eV.

The possible reaction channels are indicated as reactions **1a**-**4c** in the following:

$[CNH_3]^+ + C_2H_4 \rightarrow C_2H_5^{\bullet} + HCNH^+$ *m/z* 28 **(1a)**

$\rightarrow H_2CNH/HCNH_2 + C_2H_4^{\bullet+}$ *m/z* 28 **(1b)**

$\rightarrow C_2H_3^{\bullet} + H_2CNH_2^+$	*m/z* 30	**(2)**
$\rightarrow CH_3^{\bullet} + C_2NH_4^+$	*m/z* 42	**(3)**
$\rightarrow H^{\bullet} + CH_2CHCHNH_2^+$	*m/z* 56	**(4a)**
$\rightarrow H^{\bullet} + c\text{-}CH_2CH_2CHNH^+$	*m/z* 56	**(4b)**
$\rightarrow H^{\bullet} + CH_2NHCHCH_2^+$	*m/z* 56	**(4c)**

The reaction enthalpies estimated from literature values are summarized and compared with results from our theoretical calculations in **Table 1**

[INSERT HERE TABLE 1]

The reaction with C_2H_4 has only previously been studied with $HCNH_2^{\bullet+}$ by FT-ICR, which lead to adduct formation at *m/z* 57 plus various loss channels: of $C_2H_5^{\bullet}$ (reaction **1a**), of $NH_2^{\bullet}$ (to yield $C_3H_5^+$, *m/z* 41), and of $H^{\bullet}$ (channels **4a-b-c**)[24], with the latter being about three times more abundant than the others. This same work also examined the reaction with C_2D_4 wich showed a 27:73 ratio for the loss of H:D from the adduct equivalent to reactions **4a-c**. In our study the production of an ion at *m/z* 41 ($C_3H_5^+$) from $HCNH_2^+$ generated from cyclopropylamine is observed only at photon energies above ~12.4 eV and it is attributed to reactions of $C_2H_5^+$ contaminants (see **Supplementary Information - Part 2**). It is likely that this is also the case when $HCNH_2^+$ is formed starting from cyclopropylamine in an electron ionization source[24].

Cross sections (CSs) for the reaction of both ions as a function of the photon energy (E_{phot}) at fixed collision energy (E_{CM}) are given in **Fig. 1**, while in **Fig. 2**. CSs as a function of the collision energy are shown. In **Table 2** results obtained at a fixed E_{phot} = 11.48 eV and fixed E_{CM} =0.13 eV are summarized, by reporting the branching ratios (BRs) and the total rate constants $k_{tot}(E_{ave})$. The latter have been estimated using the expression $k_{tot}(E_{ave}) = \langle v \rangle \cdot \sigma_{tot}$, were σ_{tot} is the total reactive CS (i.e. sum over all product channels), <v> is the average relative velocity, and E_{ave} is the average energy that can be obtained from the collision energy $E_{ave} = E_{CM} + 3/2\gamma k_B T$[1] [33, 34]. The ratio between k_{tot} and the Langevin collision rate constant (k_L), also reported in **Table 2**, is a useful estimate of the overall efficiency of the reactions, which proceed at a smaller rate than the Langevin limit, namely 16% and 26% of k_L for $HCNH_2^{\bullet+}$ and $H_2CNH^{\bullet+}$ respectively.

Table 2. Total rate constants at fixed average energy $k_{tot}(E_{ave})$ and branching ratios (BRs) for the reaction of $HCNH_2^{\bullet+}$ and $H_2CNH^{\bullet+}$ with C_2H_4. Results have been obtained at fixed E_{phot} =11.48 eV and E_{CM} = 0.13±0.01 eV, corresponding to an average energy E_{ave}=0.15±0.01.

	$HCNH_2^{\bullet+}$	**$H_2CNH^{\bullet+}$**
$k_{tot}(E_{ave})$ [a]	$(2.0\pm0.5)\times10^{-10}$	$(3.3\pm0.9)\times10^{-10}$

[1] γ=0.508 is the ratio of the parent ion mass over the sum of the masses of charged and neutral reagents; k_B is the Boltzmann constant and T is the gas temperature in the scattering cell (~300 K in our set-up)

k_{tot} / k_L [b]	0.16	0.26
product (m/z)	**Branching ratios (BRs)**	
28	0.05 [c]	0.24 ± 0.11
30	0.43 ± 0.16	0.23 ± 0.10
42	0.010 ± 0.005	0.08 ± 0.03
56	0.51 ± 0.20	0.44 ± 0.18

[a] Total (i.e., summed over all the product channels) rate constant (in $cm^3 \cdot molecule^{-1} \cdot s^{-1}$) at the specified average collision energy E_{ave}, estimated as detailed in the text.
[b] For both isomers $k_L = 1.27 \times 10^{-9}$ $cm^3 \cdot molecule^{-1} \cdot s^{-1}$ is the Langevin rate constant, calculated using the value 4.188 $Å^3$ for the average electronic polarizability of C_2H_4
[c] Upper limit value

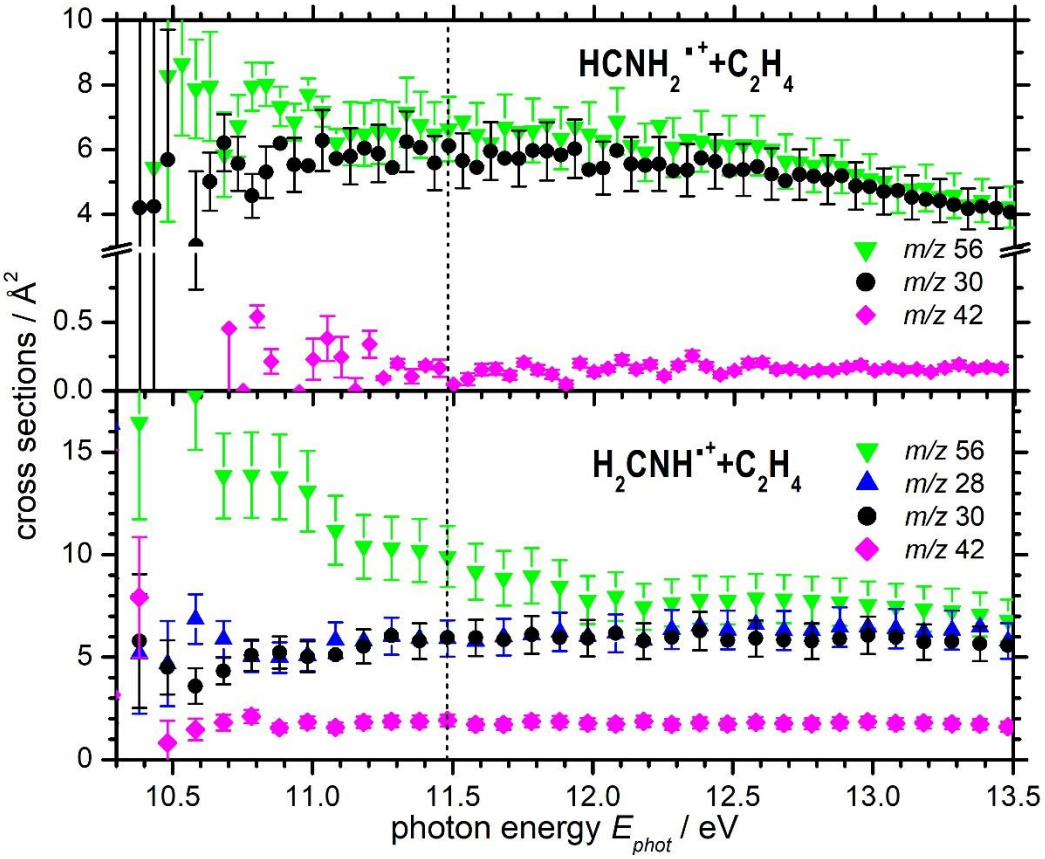

Fig. 1: Reactive cross sections as a function of E_{phot} for the reaction of $HCNH_2^{\bullet+}$ (top) and $H_2CNH^{\bullet+}$ (bottom) with C_2H_4 . Collision energies are E_{CM}=0.15 eV (top) and E_{CM}=0.13 eV (bottom). The vertical dashed lines indicate the photon energy at which data have been collected as a function of E_{CM} (see **Fig. 2**)

The *m/z* 56 product is the major one at all photon energies for both isomers. For the $HCNH_2^{\bullet+}$ isomer, this channel shows no significant dependence on E_{phot} indicating that it proceeds independently of the internal energy of the reactant ion. The decrease in CS at E_{phot} > 12.4 eV, also observed for the other major product at *m/z* 30, is an artefact due to the increasing contamination of $C_2H_5^+$ in the parent beam (see discussion in the **Supplementary Information - Part 2**), which reduces the relative amount of $HCNH_2^{\bullet+}$ ion available for reaction. The next most significant product for the $HCNH_2^{\bullet+}$ isomer is at *m/z*

30, with similar trend with E_{phot} as *m/z* 56. A minor channel at *m/z* 42 is detected and approximately constant (within uncertainty) as a function of E_{phot}.

For the $H_2CNH^{\bullet+}$ isomer, after the *m/z* 56 channel, the *m/z* 28 and 30 are the next most significant pathways, with equivalent CSs over the entire photon energy range. It is worth noting that at low photon energies the *m/z* 56 channel shows initial decrease before levelling off above 12 eV, whereas the *m/z* 30 channel undergo a slight increase over this same photon energy range. This is discussed further in **Section 5**. The minor channel at *m/z* 42 is also observed, being largely constant but notably more intense than for the other isomer.

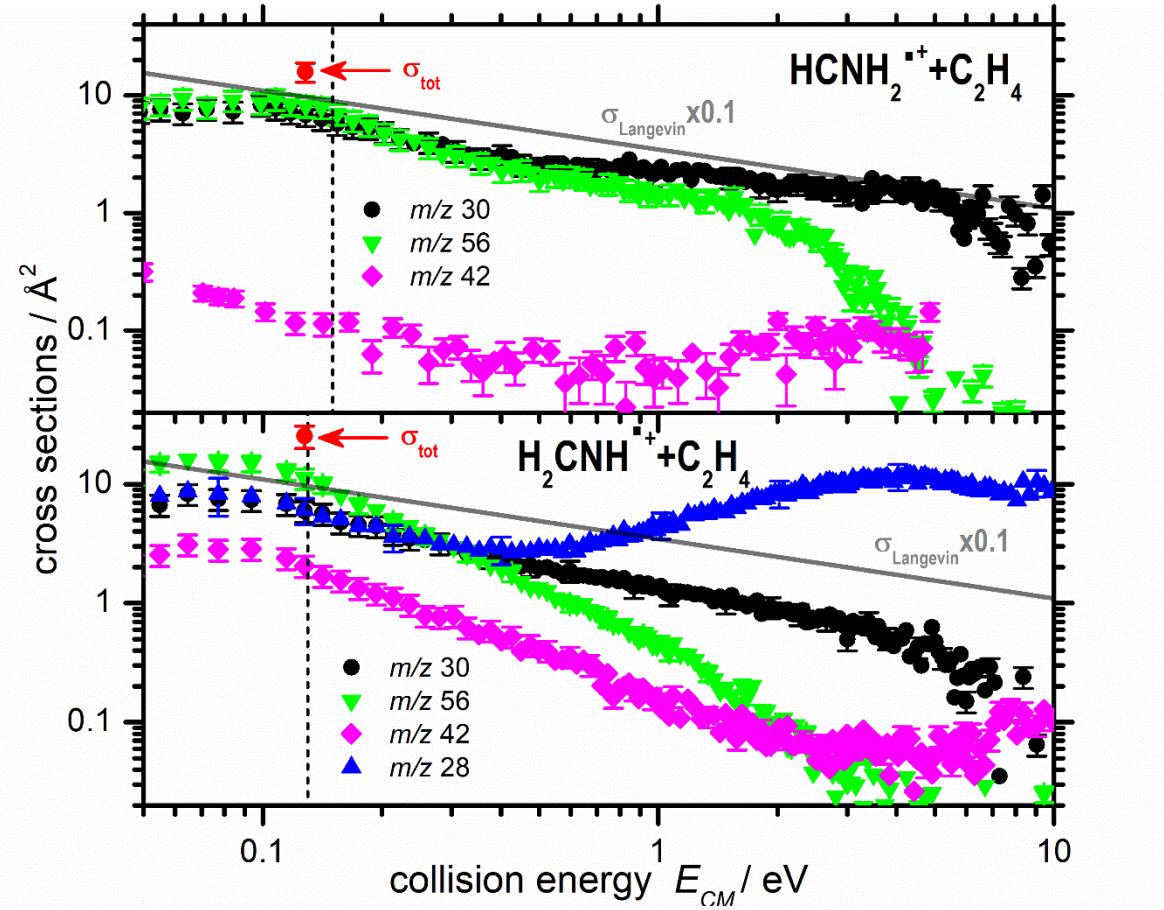

Fig. 2: Reactive cross sections as a function of the collision energy E_{cm} for the reaction of $HCNH_2^{\bullet+}$ (top) and $H_2CNH^{\bullet+}$ (bottom) with C_2H_4. The photon energy is fixed at E_{phot}=11.48 eV, with the exception of *m/z* 42 from $HCNH_2^{\bullet+}$ for which is equal to 12.48 eV. The vertical dashed lines indicate the collision energy at which data have been collected as a function of E_{phot} (see **Fig. 1**). The grey solid lines are the Langevin CSs (rescaled by a factor 0.1 to fit in the figure) that are identical for both isomers. The red points are the total reactive CSs (σ_{tot}) used to calculate the total rate constants k_{tot} reported in **Table 2**.

The trends as a function of the collision energy (**Fig. 2**) are very similar for the *m/z* 30 from both isomers, with a gradual decrease with increasing E_{CM} indicative of a barrierless exothermic process. It is worth noting that the *m/z* 30 products follow closely (at least at the

low energies) the $E^{-0.5}$ kinetic energy dependence trend represented by the Langevin capture cross sections (shown in **Fig. 2** as grey lines, rescaled by a factor 0.1 to fit in the figure). Products at *m/z* 56 from both isomers show a slightly sharper decrease with increasing collision energy, indicative of a mechanism proceeding via adduct formation. This decrease is notably sharper for the $H_2CNH^{\bullet+}$ isomer (see **Section 5** for a possible explanation).

The *m/z* 42 channel also shows a similar trend for both isomers, with a predominant low collision energy peak typical of a barrierless mechanism with a secondary rise at higher collision energies, indicating a second process involving an energy barrier. It should be noted that, while in **Fig. 2** two different E_{phot} are used for *m/z* 42 from the two isomers, the lack of photon energy dependence for this product in the explored range (see **Fig. 1**) can be used to infer that no significant change is expected when comparing data taken at different values of E_{phot} .

The *m/z* 28 product, only measured with $H_2CNH^{\bullet+}$, shows an initial decrease with increasing collision energy indicative of a barrierless process, but then displays a significant rise to a plateau. This is a strong indication of the combination of a barrierless channel with either an endothermic pathway or one having an energy barrier. A detailed discussion of the trends of all products in light of computational results is presented in **Section 5**.

4. Computational Results

In agreement with previous theoretical studies,[26,35] our calculations show that the aminocarbene ($HCNH_2^{\bullet+}$) is more stable than the methanimine radical cation ($H_2CNH^{\bullet+}$) by about 17.9 kJ·mol^{-1} and the two isomers are separated by an isomerisation barrier for 1,2-H shift of ~280 kJ·mol^{-1} (with respect to $H_2CNH^{\bullet+}$ energy). This value is substantially higher than the barrier associated to H loss from either isomer, thus making dissociation favoured over isomerization.

The two isomers are able to form both van der Waals complexes and covalently-bound adducts with ethene. In both cases, the van der Waals complex results from the approach of the ion to the neutral by the non-radical terminus, whereas the covalent adducts are formed by approach to the neutral by the radical end.

Please note that the relative enthalpies reported in the figures are given (in kJ·mol^{-1}) with respect to the sum of the energies of the separated reactants having the lowest energy (*i.e.* $HCNH_2^{\bullet+}$ plus C_2H_4). However, the reaction enthalpies of the various channels as reported in **Table 1** and in the text, are calculated with respect to the specific reactant (either $HCNH_2^{\bullet+}$ or $H_2CNH^{\bullet+}$).

$HCNH_2^{\bullet+}$ isomer (pathways are described graphically in **Fig. 3** and **4**, while reaction enthalpies are compared with literature values in **Table 1**): two different van der Waals complexes resulting from the N-terminal approach of the ion to C_2H_4 can be formed, namely **A1** and **A4**. They differ for the orientation of the H on the C atom of the ion: in **A1** the H is *Z*- to the H of the NH_2 group directed towards the π bonding system of ethene, whereas in **A4** it is *E*-. From **A1** the formation of the covalently-bound adduct **A2** proceeds via the

transition state (TS) **A1-2**. **A2** can readily eject an H via TS **A2-P** to give the *m/z* 56 product $CH_2CHCHNH_2^+$ (reaction **4a**, calculated enthalpy $\Delta H_0°$ =-112.9 kJ·mol^{-1}= -1.17 eV, see **Table 1** and **Fig. 3**). The other major product channel is the *m/z* 30 one, which can be formed in two ways. Firstly, from **A2** which undergoes an isomerization to **A3** via TS **A2-3** prior to a barrierless fragmentation into $H_2CNH_2^+$ and $C_2H_3^•$ (reaction **2**, calculated enthalpy $\Delta H_0°$ = -28 kJ·mol^{-1}= -0.29 eV, see **Table 1** and **Fig. 3**). Alternatively it can be formed via **A4**, which can transfer an H atom to give the cluster **A5** via TS **A4-5**. This species can then barrierlessly fragment to the same products.

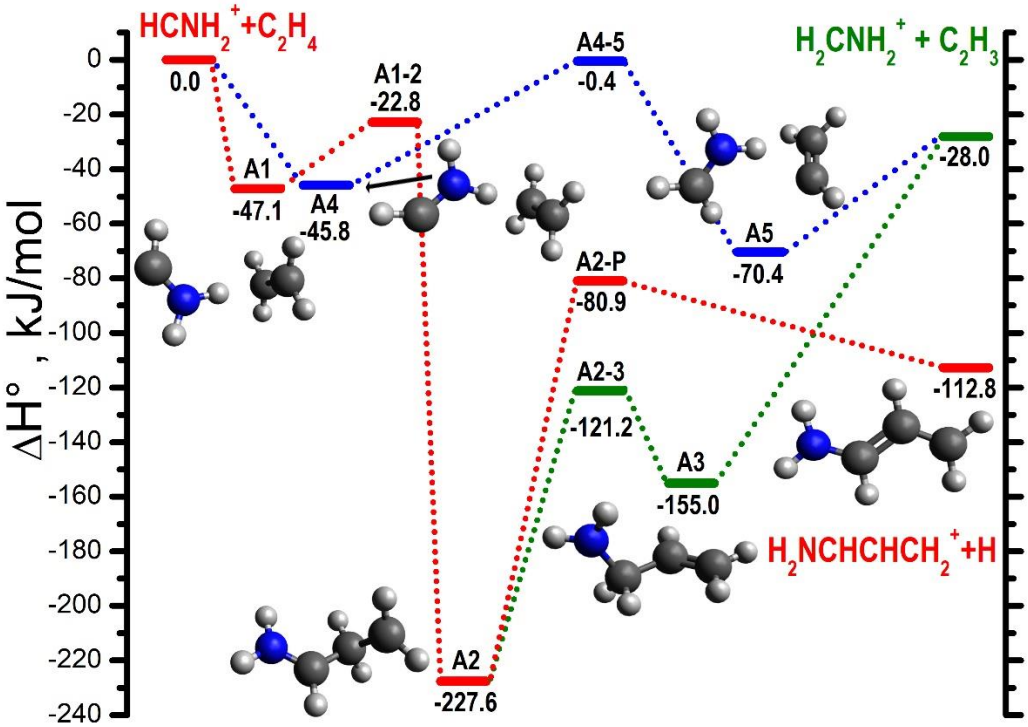

Fig. 3. ***$HCNH_2^{•+}$ plus C_2H_4***: relative enthalpies (at 0 K) and reaction pathways leading to products $H_2CNH_2^+$ plus $C_2H_3^•$ (in blue and green) and $NH_2CHCHCH_2^+$ plus $H^•$ (in red). The zero value for enthalpies (in kJ·mol^{-1}) corresponds to the separated $HCNH_2^{•+}$ plus C_2H_4 reactants. Calculations are at the MP2/cc-pVTZ//CCSD(T)/cc-pVTZ level of theory. Ball-and-stick structures refer to stable intermediates, whereas TS structures are given in the **Supplementary Information - Part 1.**

The formation of the *m/z* 42 product from $HCNH_2^{•+}$ can proceed from **A2** via TS **A2-6** to give **A6**. This can rearrange to **A7** via TS **A6-7**. **A7** can then transform, via TS **A7-8**, to **A8** which subsequently fragments barrierlessly to give protonated ketenimine ($CH_2CNH_2^+$) plus $CH_3^•$ (reaction **3**, calculated enthalpy $\Delta H_0°$ =-51.2 kJ·mol^{-1}= -0.53 eV, see **Table 1** and **Fig. 4**). Although we have not measured the E_{phot} and E_{CM} trends of the CSs for the *m/z* 28 product from this isomer as the signal was too minor to make it separatable from the parent beam, a submerged pathway for its formation is here presented. **A2** can convert into its rotamer **A9** via TS **A2-9**. **A9** can undergo a [1,4] H shift to give **A10** via TS **A9-10**. **A10** can then convert into the rotamer **A11** via TS **A10-11**. In turn, **A11** can cleave the central C-C

bond to form **A12**, a complex of $HCNH^+$ and $C_2H_5^{\bullet}$, via TS **A11-12**. This complex can barrierlessly fragment to give products (reaction **1a,** calculated enthalpy $\Delta H_0°$ = -21.7 kJ·mol^{-1}= -0.22 eV, see **Table 1** and **Fig. 4**).

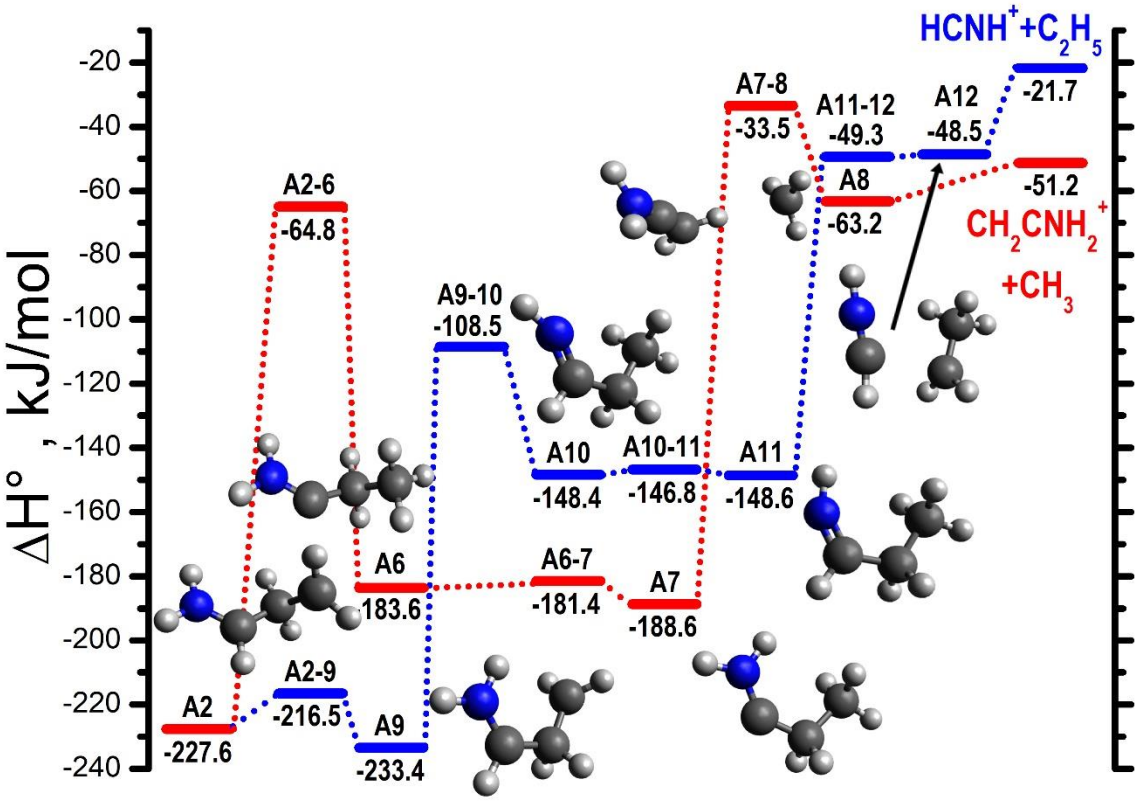

Fig. 4. ***$HCNH_2^{\bullet+}$ plus C_2H_4***: relative enthalpies (at 0 K) and reaction pathways leading to products $HCNH^+$ plus $C_2H_5^{\bullet}$ (in blue) and $CH_2CNH_2^+$ plus $CH_3^{\bullet}$ (in red). The zero value for enthalpies (in kJ·mol^{-1}) corresponds to the separated $HCNH_2^{\bullet+}$ plus C_2H_4 reactants. Calculations are at the MP2/cc-pVTZ//CCSD(T)/cc-pVTZ level of theory. Ball-and-stick structures refer to stable intermediates, whereas TS structures are given in the **Supplementary Information - Part 1.**

$H_2CNH^{\bullet+}$ isomer (pathways are described graphically in **Fig. 5** and **6**, while reaction enthalpies are compared with literature values in **Table 1**): the covalently bound adduct **B1** is formed barrierlessly. From **B1** two pathways are possible to form different isomeric products at *m/z* 56. In one case **B1** can rearrange into its rotamer **B2** via TS **B1-2**. This can then eject an H to form $CH_2NHCHCH_2^+$ via TS **B2-P** (reaction **4c**, calculated enthalpy $\Delta H_0°$ = -76.3 kJ·mol^{-1}= -0.79 eV, see **Table 1** and **Fig. 6**). An alternative pathway proceeds through **B1** cyclisation to give **B3** via TS **B1-3.** This can then eject a H to give c-$CH_2CH_2CHNH^+$ via TS **B3-P** (reaction **4b**, calculated enthalpy $\Delta H_0°$ =-69.2 kJ·mol^{-1}= -0.72 eV, see **Table 1** and **Fig. 5**).

The $H_2CNH^{\bullet+}$ isomer also has two possible mechanisms for formation of products at *m/z* 30 amu, though only one is fully submerged. This pathway proceeds via the van der Waals complex **B4** (see **Fig. 5**) and involves an H transfer from C_2H_4 to the ion to give structure

A5 (already mentioned in the reactivity of $HCNH_2^{\bullet+}$, see **Fig. 3**) via TS **B4-A5**. **A5** can barrierlessly separate to form $H_2CNH_2^+$ plus $C_2H_3^\bullet$ (reaction **2**, calculated enthalpy $\Delta H_0° = -45.9$ kJ·mol^{-1}= -0.48 eV, see **Table 1** and **Fig. 6**). The other mechanism requires the rearrangement of **B2** into **B5**, an isomerisation that is hampered by a barrier of 28 kJ·mol^{-1} above reagents going via TS **B2-5**. Subsequently, the barrierless rupture of the C-N bond in **B5** leads to products (see **Fig. 6**).

The formation of the other major product at *m/z* 28 first involves a [1,4] H shift from **B1** to give **B6** via TS **B1-6**. **B6** can then rearrange to form its rotamer **B7** via TS **B6-7**. This can then cleave the central C-N bond to give **B8**, a van der Waal complex of $HCNH^+$ and $C_2H_5^\bullet$ via TS **B7-8**. **B8** can then separate barrierlessly to give products $HCNH^+$ plus $C_2H_5^\bullet$ (reaction **1a**, calculated enthalpy $\Delta H_0° = -39.6$ kJ·mol^{-1}= -0.41 eV, see **Table 1** and **Fig. 5**).

The mechanism for formation of *m/z* 42 product proceeds from **B2** via TS **B2-9** to give **B9**. This can then transform to its rotamer **B10** via TS **B9-10** which in turn can fragment via TS **B10-P** to give $CH_2NCH_2^+$ and $CH_3^\bullet$ (reaction **3**, calculated enthalpy $\Delta H_0° = -67.1$ kJ·mol^{-1}= -0.70 eV, see **Table 1** and **Fig. 6**).

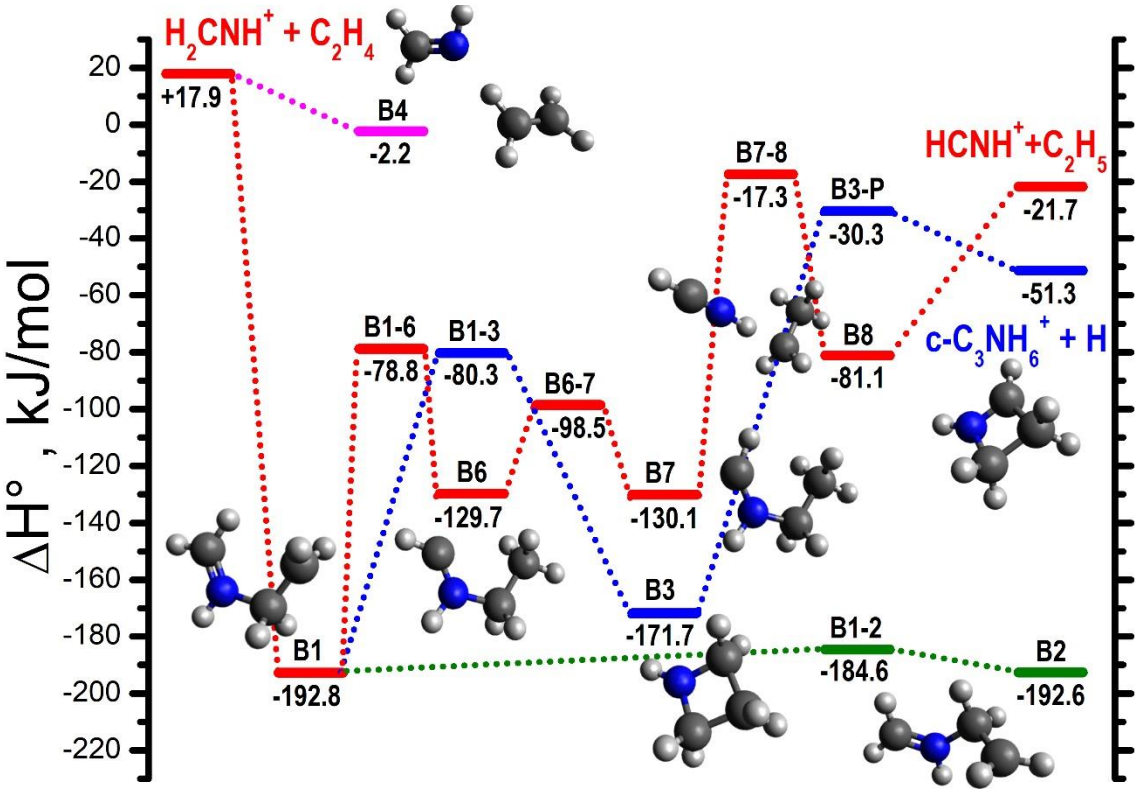

Fig. 5. ***$H_2CNH^{\bullet+}$ plus C_2H_4***: relative enthalpies (at 0 K) and reaction pathways leading to products $HCNH^+$ plus $C_2H_5^-$ (in red) and c-$CH_2CH_2CHNH^+$ plus H^- (in blue). The zero value for enthalpies (in kJ·mol^{-1}) corresponds to the separated $HCNH_2^{\bullet+}$ plus C_2H_4 reactants (same **as Fig. 3** and **4**). Calculations are at the MP2/cc-pVTZ//CCSD(T)/cc-pVTZ level of theory. Ball-and-stick structures refer to stable intermediates, whereas TS structures are given in the **Supplementary Information - Part 1.**

5. Discussion

The chemistry of $HCNH_2^{\bullet+}$ is dominated by processes involving the formation of intermediate adducts, with all three main channels proceeding at least partly in this way. However, the *m/z* 30 channel may proceed additionally via a direct H atom transfer, as discussed in the accompanying paper [16]. The *m/z* 56 channel is expected to be the major product going via an adduct pathway as this is the most exothermic channel and only involves a couple of rearrangements (from the initial van der Waals cluster **A1** to **A3**) for formation. It is therefore the most favoured channel both kinetically and thermodynamically.

For $H_2CNH^{\bullet+}$, the decrease in the *m/z* 56 product with increasing collision energy is more pronounced. This difference can be attributed to the fact that the lowest energy pathway proceeds via a cyclisation, which is likely to be sterically inhibited by increasing the collision energies, whereas this is not the case for $HCNH_2^{\bullet+}$ where the H ejection pathway proceeds via open structures. A similar explanation holds for the slight decrease in CS as the photon energy (and by extension the internal energy of the $H_2CNH^{\bullet+}$ reactant) is increased, since internal energy inhibits the cyclisation, and while there is a direct ejection pathway with submerged barriers (see **Fig. 6**), this involves higher barriers than the pathway via the cyclised adduct.

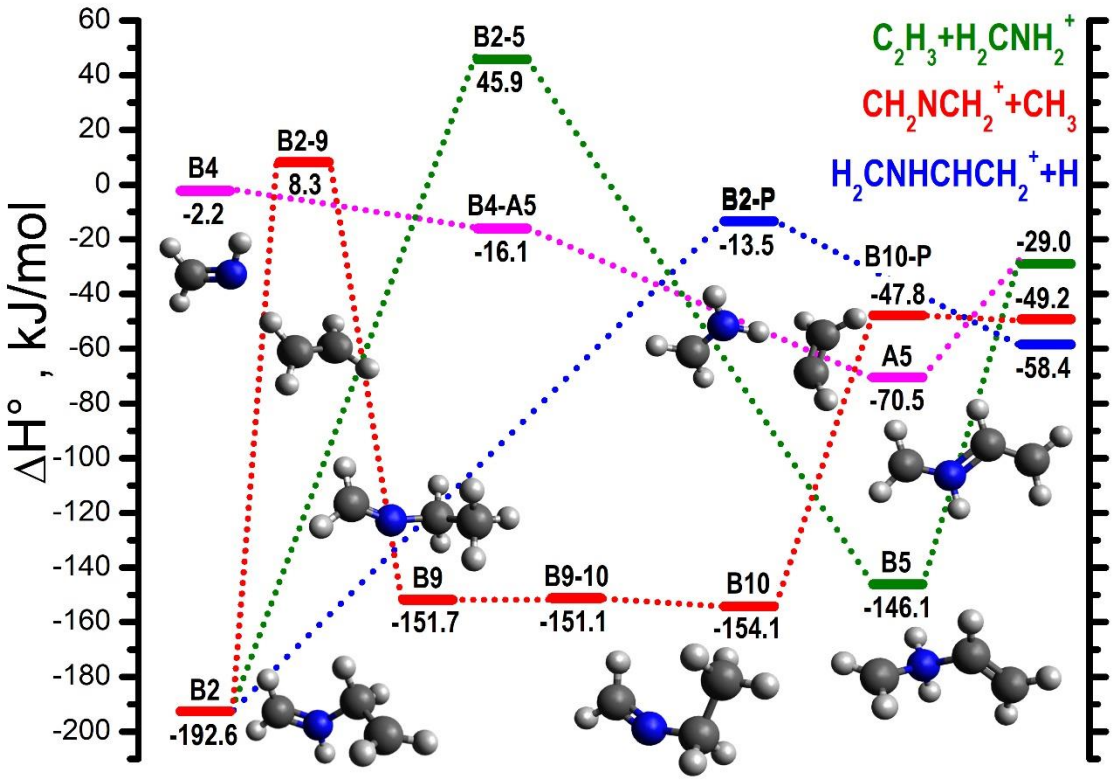

Fig. 6. ***$H_2CNH^{\bullet+}$ plus C_2H_4***: relative enthalpies (at 0 K) and reaction pathways leading to products $CH_2CNH_2^+$ plus $CH_3^{\bullet}$ (in red), $H_2CNH_2^+$ plus $C_2H_3^{\bullet}$ (in green and pink) and $CH_2NHCHCH_2^+$ plus $H^{\bullet}$ (in blue). The zero value for enthalpies (in $kJ \cdot mol^{-1}$) corresponds to the separated $HCNH_2^{\bullet+}$ plus C_2H_4 reactants (same as Figs. 3-5). Calculations are at the MP2/cc-pVTZ//CCSD(T)/cc-pVTZ level of theory. Ball-and-stick

structures refer to stable intermediates, whereas TS structures are given in the **Supplementary Information - Part 1.**

Interestingly, calculations predict different structures for the $C_3H_6N^+$ products from the two isomers. For $HCNH_2^{\bullet+}$, adduct formation proceeds through C-C bond formation, thereby leading to the most stable $C_3H_6N^+$ isomer, $CH_2CHCHNH_2^+$ (reaction **4a**, see **Table 1**). On the other hand, the radical character of the N-H terminal of the methanime radical cation leads to C-N bond formation, which favours the production of the higher energy $C_3H_6N^+$ isomers c-$CH_2CH_2CHNH^+$ and $CH_2NHCHCH_2^+$. The formation of other isomers with *m/z* 56 cannot be excluded, but a discusson of those is beyond the scope of this study.

The *m/z* 30 channel can proceed either via the covalently bound adducts or via van der Waals complexes with ethene, as well as likely exhibiting some contribution from a direct H-stripping process (see the discussion on the H atom transfer reaction with CH_4[16]). The collisional energy dependence of the CS is very similar for the two isomers, showing only a slightly more significant decrease with increasing collision energy for $H_2CNH^{\bullet+}$, likely due to the competition with the *m/z* 28 channel, which is smaller for the $HCNH_2^{\bullet+}$ isomer.

The *m/z* 28 channel shows the most significant differences between the two isomers. At low collision energies there is a fully-submerged adduct pathway to form this product with both isomers, but for $HCNH_2^{\bullet+}$ this involves significantly more rearrangement and so is kinetically more inhibited, which may explain the smaller CS (by about a factor 7) for this channel at low collision energies. At high collision energies, the $H_2CNH^{\bullet+}$ isomer shows a marked increase followed by a plateau, which is expected to correspond to the endothermic charge transfer channel (reaction **1b**, calculated enthalpy ΔH_0° =+53.0 kJ·mol^{-1}= +0.55 eV), which opens up at high collision energies, thus leading to the observed double-bell effect. It should be noted that with increasing kinetic energy of the parent ion, a contribution at *m/z* 28 may also come from collision induced dissociation of the latter to give $HCNH^+$ plus H which requires at least 1.3 eV of energy for the $H_2CNH^{\bullet+}$ isomer.
The *m/z* 42 channel is minor but present for both isomers. For $HCNH_2^{\bullet+}$, there is a barrierless pathway via adduct formation, with the small CS being attributed to the fact that it requires multiple rearrangements. For $H_2CNH^{\bullet+}$, the pathway also proceeds barrierlessly via formation of a covalently bound adduct; it is thermodynamically favoured, though as it also requires a number of rearrangements it is far more kinetically inhibited than the two major channels.

Importantly, present results from the reactivity with C_2H_4 demonstrate better than reactivity with CH_4 (see our accompanying paper [16]) that the two radical cation isomers have markedly different chemistries. This is a strong evidence in support of the selectivity of our ion generation processes and of the fact that reagent ion isomerization prior to reaction is not occurring under our experimental conditions.

6. Conclusions

The reaction of the methanimine radical cation ($H_2CNH^{\bullet+}$) and its isomer aminomethylene ($HCNH_2^{\bullet+}$) with C_2H_4 is reported by measuring the dependence on both photon and collision

energies of the product CSs (in absolute values) using a guided ion beam tandem mass spectrometer with VUV dissociative ionization for ion generation. The different behaviour of products clearly show that it is possible to produce the different isomers selectively through the choice of suitable precursor molecules. It also shows that isomerisation reactions of the reactants do not occur in the present set-up. Experimental results are rationalized via reaction mechanisms proposed on the basis of ab initio calculations of the most relevant stationary points on the potential energy surfaces.

For both isomers, the channel leading to a *m/z* 56 is the primary product at low collision energies and calculations indicate that: *a)* it may proceed via H-elimination from an initially formed adduct and *b)* the structure of products is influenced by the structure of the cationic isomer. The title reactions can therefore serve as intermediate steps to form larger nitrogen-containing species in different ionic environments, including Titan's atmosphere. The channel leading to *m/z* 30 (formation of $CH_2NH_2^+$) is also prominent for both isomers, whereas the product at *m/z* 42 (elimination of a methyl radical from the adduct) is a minor feature, especially in the case of $HCNH_2^{\bullet+}$. A key difference between the reactivity of the two isomers is the product at *m/z* 28 ($HCNH^+$) which has a cross section ~ 7 times smaller in $HCNH_2^{\bullet+}$ compared to $H_2CNH^{\bullet+}$, at least at low collision energies. All observed channels show a negative dependence of the cross sections on the collision energies at low E_{CM} (smaller than 0.5 eV) which points to exoergic and barrierless processes which are feasible in cold environments like the interstellar medium and Titan's atmosphere.

Acknowledgements

We are grateful to the DESIRS beamline team for their assistance during the synchrotron measurements and to the technical staff of SOLEIL for the smooth running of the facility under projects n◦ 20180118 and 20190249. This work was supported by the European Union's Horizon 2020 research and innovation programme "Astro-Chemistry Origins" (ACO), Grant No 811312. W.G. thanks the Swedish Research Council for a project grant (grant number 2019-04332). M.P. and J.Ž. acknowledge support from the Ministry of Education, Youth and Sports of the Czech Republic (grant No. LTC20062). V.R. acknowledges funding for a PhD fellowship from the Dept. Physics, University of Trento.

Bibliography

[1] M Larsson,. W. Geppert, G. Nyman, Rep. Prog. Phys. 75 (2012) 066901
[2] R. C. Woods, C. S. Gudeman, R. L. Dickman, P. F. Goldsmith, G. R. Huguenin, W. M. Irvine, Å. Hjalmarson, L.-Å. Nyman, and H. Olofsson, Astrophys. J. 270 (1983) 583-588
[3] M. A. Cordiner, N. A. Teanby, C. A. Nixon, V. Vuitton, A. E. Thelen, S. B. Charnley, Astronomical Journal, 158 (2019) 76
[4] P.Fathi, W. D. Geppert, A.Kaiser, D.Ascenzi, Mol. Astrophys. 2, (2016) 1-11
[5] M. Polášek, E.-L. Zins, C. Alcaraz, J. Zabka, V. Krizova, L.Giacomozzi, P. Tosi, D, Ascenzi J. Phys. Chem. A 120 (2016) 5041-5052
[6] S. Brunken, F. Lipparini, A. Stoffels, P. Jusko, B. Redlich, J. Gauss, S. Schlemmer, J. Phys. Chem. A, 123 (2019) 8053-8062
[7] S. Hörst, J. Geophys. Res. Planets, 122 (2017) 432–482
[8] S. Vinatier, B. Bezard, Icarus 2007188 (2007)120–138
[9] C.A. Nixon, R.D. Lorenz, R.K. Achterberg et al. Plan. Space Sci. 155 (2018) 50–72

[10] H. Imanaka,H., M. A. Smith, ,Geophys. Res. Lett. 34 (2007) L02204.
[11] E. Vigren, J.Semaniak, M. Hamberg, V. Zhaunerchyk M. Kaminska R.D. Thomasa, M. af Ugglas, M. Larsson, W.D. Geppert, Planet. Space Sci. 60 (2012) 102
[12] J.H. Westlake, J.H. Waite, N. Carrasco, M. Richard, T. Cravens, J. Geophys. Res. A119 (2014) 5951–5963
[13] V. Vuitton, R.V. Yelle, S.J. Klippenstei, S.M. Hörst, P. Lavvas, Icarus 324 (2019) 120–197
[14] J.H. Waite, D.T. Young, T.E. Cravens, A.J. Coates, F.J. Crary, B. Magee, J. Westlake, Science 316 (2007) 870-875
[15] V. Vuitton, R.V. Yelle, M.J. McEwan, Icarus 191 (2007) 722–742.
[16] V. Richardson, C. Alcaraz, W. Geppert, J.-C. Guillemin, M. Polášek, C. Romanzin, D. Sundelin, R. Thissen, P. Tosi, J. Žabka, D. Ascenzi *Chem.Phys.Lett. (2021), accepted for publication*
[17] C. Alcaraz, C. Nicolas, R. Thissen, J. Žabka, and O. Dutuit, J. Phys. Chem. A 108 (2004) 9998–10009
[18] B. Cunha de Miranda, C. Romanzin, S. Chefdeville, V. Vuitton, J. Žabka, M. Polášek et al. , J. Phys. Chem. A 119 (2015) 6082–6098
[19] L. Nahon, N. de Oliveira, G.A. Garcia, J-F. Gil, B. Pilette, O. Marcouillé, B. Lagarde, and F. Polack, J. Synchrotron Rad. 19 (2012) 508–520
[20] E. Teloy, D. Gerlich, Chem. Phys. 4 (1974) 417 – 427
[21] M. J. Frisch, G. W. Trucks, H. B. Schlegel et al., Gaussian 09, Revision D.01, Gaussian, Inc., Wallingford CT, 2013
[22] M.J. Polce Y. Kim, C. Wesdemiotis Int. J. Mass Spectrom. Ion Proc167/168 (1997) 309-315
[23] P.C. Burgers, J.L. Holmes and J.K. Terlouw, J. Am. Chem. Soc. 106 (1984) 2762
[24] J. Chamot-Rooke, P. Mourgues, G. van der Rest, H.E. Audier, Int. J. Mass Spectrom. 226 (2003) 249–269
[25] V. G. Anicich, JPL-Publication-03-19 (2003) http://hdl.handle.net/2014/7981
[26] M.T. Nguyen, J. Rademakers, J.M.L. Martin, Chem. Phys. Lett. 221(1994) 149
[27] NIST ChemistryWebBook, NIST Standard Reference Database Number 69 (2018), Available: https://webbook.nist.gov/chemistry/ eds. P.J. Linstrom, and W.G. Mallard (Gaithersburg, MD: National Institute of Standards and Technology), 20899.
[28] J. Holmes, C. Aubry, and P. Mayer, Assigning Structures to Ions in Mass Spectrometry (2006) CRC Press, Taylor & Francis Group, Boca Raton FL (USA)
[29] J. Holmes, F.P. Lossing and P.M. Mayer, Chem. Phys. Lett. 198 (1992) 211-213
[30] A.K. Eckhardt and P.R. Schreiner, Angew. Chem. Int. Ed. 57 (2018) 5248 –5252
[31] Z. A. Harvey, J. C. Traeger Eur. J. Mass Spectrom. 10 (2004) 759–765 https://doi.org/10.1255/ejms.681
[32] G. Bouchoux, B. Gaudin, D. Leblanc, M. Yáñez and O. Mó, Int. J. Mass Spectrom. 199 (2000) 59–69. https://doi.org/10.1016/S1387-3806(00)00190-1
[33] new K. M. Ervin, P.B. Armentrout, J. Chem. Phys. 83, (1985) 166–189. doi: 10.1063/1.449799
[34] C. Nicolas, C. Alcaraz, R. Thissen, J. Žabka, and O. Dutuit, Plan. Space Sci. 50 (2002) 877–887. doi: 10.1016/S0032-0633(02)00063-6
[35] J. Zhou and H. B. Schlegel, J. Phys. Chem. A 113 (2009) 9958–9964.

The reactivity of methanimine radical cation ($H_2CNH^{\bullet+}$) and its isomer aminomethylene ($HCNH_2^{\bullet+}$) with C_2H_4

D. Sundelin[a], D. Ascenzi[b], V. Richardson[b], C. Alcaraz[c,d], M. Polášek[e], C. Romanzin[c,d], R. Thissen[c,d], P. Tosi[b], J. Žabka[e] and W. Geppert[a *]

[a] Department of Physics, Stockholm University, Roslagstullsbacken 21, 10691 Stockholm, Sweden

[b] Department of Physics, University of Trento, Via Sommarive 14 – 38123 Italy

[c] Université Paris-Saclay, CNRS, Institut de Chimie Physique, UMR8000, 91405 Orsay, France

[d] Synchrotron SOLEIL, L'Orme des Merisiers, F-91192 Saint Aubin, Gif-sur-Yvette, France

[e] J. Heyrovsky Institute of Physical Chemistry of the Czech Academy of Sciences, Dolejškova 3, Prague 8, 18223 Czech Republic

* corresponding author: e-mail wgeppert@fysik.su.se phone: ++ 46 8 5537 8649

Keywords: interstellar medium; rate constant; ion-molecule reactions; astrochemistry molecular astrophysics; isomerism; Titan's atmosphere; protonated ketenimine

Graphical abstract

Abstract

Experimental and theoretical studies are presented on the reactivity of $H_2CNH^{\bullet+}$ (methanimine) and $HCNH_2^{\bullet+}$ (aminomethylene) with ethene (C_2H_4). Selective isomer generation is performed via dissociative photoionization of suitable neutral precursors and reactive cross sections and branching ratios are measured as a function of photon and collision energies. Differences between isomers' reactivity are discussed in light of *ab-initio* calculations on reaction mechanisms. The main products, for both isomers, are H-elimination, most likely occurring from covalently bound adducts (giving c-$CH_2CH_2CHNH^+$/$CH_2NHCHCH_2^+$) and $H^{\bullet}$ atom transfer to yield $H_2CNH_2^+$. The astrochemical implications of the results are briefly addressed.

1. Introduction

Ion-induced processes have long been regarded as playing a pivotal role in the synthesis of complex molecular species in the interstellar medium, as well as the atmospheres of planets and their satellites[1]. Increasingly complex ions have been detected using state-of-the-art terrestrial single-dish telescopes and interferometers, and with this increase in complexity the role of isomers becomes crucial. Isomers have different spectroscopic and chemical properties and, since isomerisation barriers for many species are too high to be overcome thermally under interstellar conditions, they have to be treated as different species with distinctive chemical reactivities in astrochemical models. The existence of

isomeric ions in the interstellar medium has long been known, and in the case of HCO^+ and HOC^+ their relative abundance ratio has been assessed[2] allowing conclusions to be drawn about the chemistry of their environments.

Whereas ionic isomers often possess different dipole moments and other spectroscopic properties, and so can be distinguished in radioastronomic observations[2], assessment of ion abundances in planetary and satellite atmospheres often relies on mass spectrometers, which cannot distinguish between isomers. As a result, their relative abundances often remain elusive in those environments. However, the novel Atacama Large Interferometer Array (ALMA) allows for the collection of column density information as a function of altitude for HCN and HNC[3]. The unprecedented resolution of ALMA will also permit the retrieval of data about the abundance and distribution of isomeric ions in different astronomic environments. In order to perform model calculations rationalising these abundances, it is important to assess the reactivity of ionic isomers with common interstellar and atmospheric molecules.

In recent years, studies have been undertaken using suitable precursor molecules to either purely or preferentially produce a single isomer [4]. VUV photoionisation has proven to be an especially versatile tool for selective production of isomers[5] while noble gas tagging has also been successfully employed to characterise isomeric ions and to determine their relative abundance after electron ionisation using different neutral precursors[6].

Titan is one of the most interesting objects in the solar system as it possesses a dense nitrogen-dominated atmosphere[7] similar to our own planet. The ion and neutral mass-spectrometer (INMS) onboard the Cassini spacecraft dicovered that Titan's atmosphere is one of the most complex in the solar system, containing large hydrocarbons and nitrogen-bearing compounds[8, 9]. This varied chemistry originates from the dissociation of its main components N_2 and CH_4 by either extreme ultraviolet (EUV) radiation[10] or magnetospheric electrons. The resultant ions and radicals can subsequently undergo ion-neutral and radical-neutral reactions leading to more complex compounds[11, 12]. Ion-neutral pathways involving unsaturated hydrocarbons (*e.g.* ethyne and ethene) in particular are frequently held responsible for the production of complex ions detected in Titan's atmosphere[12, 13]. Positive ions with masses up to 99 amu were detected by INMS at altitudes of 950 km above the surface and the presence of cations with higher masses (up to 350 amu) were observed with the Cassini plasma spectrometer ion beam sensor (CAPS-IBS)[14]. It is therefore important to investigate the production routes of these species and the reaction of nitrogen-containing ions with hydrocarbons could play a decisive role in that. However, many of these species are protonated nitriles which are comparatively unreactive and mostly destroyed by dissociative recombination in Titan's atmosphere[15]. Contrastingly, $H_2CNH^{\bullet+}$ and its isomer $HCNH_2^{\bullet+}$ are reactive radical cations and could act as a template for the formation of larger neutral molecules through chain elongation reactions with unsaturated and saturated hydrocarbons followed by dissociative recombination of the resulting cations.

Although the mass signal at *m/z* 29 recorded by INMS can largely be attributed to a mixture of $C_2H_5^+$ and $H^{13}CNH^+$ ions, model calculations predict a density of $HCNH_2^{\bullet+}$ and its isomers

amounting to 1.1 × 10^{-2} cm^{-3} in Titan's ionosphere[15]. These species may therefore play a role in the build-up of larger nitrogen-containing species which can then further react to form aerosols associated with Titan's orange-coloured haze. This paper presents a reactivity study of $H_2CNH^{\bullet+}$ and its isomer $HCNH_2^{\bullet+}$ with ethene using synchrotron radiation and suitable precusors to selectively generate the charged species.

2. Methodology

The experimental and theoretical methodologies used have already been decribed in detail in an accompanying paper to this Special Issue devoted to reactivity of the title ions with C_2H_4 [16] as well as in Ref. [17], so only the briefest of summaries is given here.

2.1 Experimental Set-Up

Experiments were performed using the CERISES apparatus[17,18], at the DESIRS beamline[19] of the SOLEIL synchrotron radiation facility. CERISES is a guided ion beam tandem mass spectrometer composed of two octopoles located between two quadrupole mass filters. $[H_3CN]^{\bullet+}$ isomers were produced by dissociative photoionization (in the photon energy range E_{phot} = 9.5-13.5 eV) of gaseous precursors (see **Section 2.3**) introduced into the ion source at roughly 10^{-6} mbar. Ethene was introduced into the reaction cell (surrounding the first octopole) at a dynamic pressure of 2.6 x10^{-7} bar, which guarantees operation close to a single collision regime, reduces secondary reactions and limits the parent ion attenuation to less than 10%. Collision energies in the lab depend on the ion charge and on the difference between the ion source and reaction cell potentials. The retarding potential method[20] was used to determine the point which corresponds to the maximum of the first derivate of the parent ion yield, which in turn defines the zero point of the kinetic energy. The parent beam FWHM is 400 mV, which corresponds to 0.196 eV in the centre-of-mass frame. By changing the potentials of the reaction cell and all subsequent elements up to 20V, the collision energy (E_{CM}) can be increased up to 9.82 eV in the centre-of-mass frame.

2.2 Theoretical Methodology

The reaction mechanisms for both isomers were studied using GAUSSIAN[21]. Intermediate structures were calculated at the MP2/6-31G*, MP2/6-311++G** and MP2/cc-pVTZ level and the identities of transition states and minima were checked by frequency calculations and zero-point energy corrections were applied to the resultant energies. IRC calculations were performed at the MP2/6-31G* level to ensure that the transition states connect the correct minima. The dissociation pathways were probed through relaxed potential energy surface scans along the dissociation coordinates of the corresponding minima. In some cases it was necessary to fix one or two angles and a dihedral angle including the dissociating bond to avoid the scan leading to another adduct. Single point energy calculations were carried out for all stationary points at the CCSD(T)/6-311++G**and CCSD(T)/cc-pVTZ levels with zero-point energy corrections taken from the MP2/6-

311++G** and MP2/cc-pVTZ levels, respectively. In both cases the geometries were optimised at the MP2/cc-pVTZ level. Full results are given in the **Supplementary Information - Part 1.**

2.3 Ions generation and checks on impurities

The generation of the two ions through dissociative photoionization of different neutral precursors is described elsewhere[16]. Due to lack of space, the reader is referred to such references and to the **Supplementary Information - Part 2** of this work for a detailed discussion of the potential impact of isobaric impurities ($C_2H_5^+$, $H^{13}CNH^+$ and $^{13}CCH_4^{\bullet+}$) on the reaction with C_2H_4. Only the main conclusions are reported here.

The $HCNH_2^{\bullet+}$ and $H_2CNH^{\bullet+}$ isomers are generated from dissociative photoionization of cyclopropylamine (*c*-$C_3H_5NH_2$) and azetidine (c-$CH_2CH_2CH_2NH$)[22, 23, 24] respectively. In both cases the experimental appearance energies of fragments at *m/z* 29 are 10.2±0.1 eV[16]. Theoretical calculations, control experiments performed by mass selecting parent ions at *m/z* 28 from both azetidine and cyclopropylamine and literature data on the reactivity of $C_2H_5^+$, $C_2H_4^+$ and $HCNH^+$ with C_2H_4 [25] allowed us to conclude that:

a) dissociative photoionization of cyclopropylamine at photon energies above ~12.4 eV leads to contamination from $C_2H_5^+$ which can react with C_2H_4 to give $C_3H_5^+$ (*m/z* 41). This contamination channel seems less relevant in the azetidine case.
b) although the production of $HCNH^+$ from dissociative photoionization of both precursors has similar appearance energies to $HCNH_2^{\bullet+}$/$H_2CNH^{\bullet+}$ [16], the reaction of $HCNH^+$ with C_2H_4 is endothermic and leads exclusively to the proton transfer product $C_2H_5^+$. We therefore expect any contamination from $H^{13}CNH^+$ in the reagent beam not to interfere with the results discussed in the following.
c) dissociative photoionization of azetidine at photon energies above ~11.3 eV leads to a small contamination from $C_2H_4^{\bullet+}$ which can react with C_2H_4 to give $C_3H_5^+$ (*m/z* 41) plus a minor amount of $C_4H_7^+$ (*m/z* 55). However, since the ratio of the photodissociation yields for *m/z* 28 and 29 at the explored photon energies is in the range 0.3-1.0, we expect a small contamination of $^{13}CCH_4^{\bullet+}$ in the reagent beam, which may be responsible of the small signal observed at *m/z* 41 but does not interfere with the results presented here.

3. Results and discussion: reactivity experiment

The reaction of both isomers yielded products at *m/z* 30, 42 and 56 with the reaction of $H_2CNH^{\bullet+}$ also showing a product at *m/z* 28 significant enough to be separated from the parent signal. This is not the case for the $HCNH_2^{\bullet+}$ for which only an upper limit of ~0.8 Å^2 for the cross section of *m/z* 28 product could be estimated from a mass spectrum taken at E_{CM}=0.13 eV and E_{phot}=11.48 eV.

The possible reaction channels are indicated as reactions **1a**-**4c** in the following:

$[CNH_3]^+ + C_2H_4 \rightarrow C_2H_5^{\bullet} + HCNH^+$ *m/z* 28 **(1a)**

$\rightarrow H_2CNH/HCNH_2 + C_2H_4^{\bullet+}$ *m/z* 28 **(1b)**

$\rightarrow C_2H_3^{\bullet} + H_2CNH_2^+$	*m/z* 30	**(2)**
$\rightarrow CH_3^{\bullet} + C_2NH_4^+$	*m/z* 42	**(3)**
$\rightarrow H^{\bullet} + CH_2CHCHNH_2^+$	*m/z* 56	**(4a)**
$\rightarrow H^{\bullet} + c\text{-}CH_2CH_2CHNH^+$	*m/z* 56	**(4b)**
$\rightarrow H^{\bullet} + CH_2NHCHCH_2^+$	*m/z* 56	**(4c)**

The reaction enthalpies estimated from literature values are summarized and compared with results from our theoretical calculations in **Table 1**

[INSERT HERE TABLE 1]

The reaction with C_2H_4 has only previously been studied with $HCNH_2^{\bullet+}$ by FT-ICR, which lead to adduct formation at *m/z* 57 plus various loss channels: of $C_2H_5^{\bullet}$ (reaction **1a**), of $NH_2^{\bullet}$ (to yield $C_3H_5^+$, *m/z* 41), and of $H^{\bullet}$ (channels **4a-b-c**)[24], with the latter being about three times more abundant than the others. This same work also examined the reaction with C_2D_4 wich showed a 27:73 ratio for the loss of H:D from the adduct equivalent to reactions **4a-c**. In our study the production of an ion at *m/z* 41 ($C_3H_5^+$) from $HCNH_2^+$ generated from cyclopropylamine is observed only at photon energies above ~12.4 eV and it is attributed to reactions of $C_2H_5^+$ contaminants (see **Supplementary Information - Part 2**). It is likely that this is also the case when $HCNH_2^+$ is formed starting from cyclopropylamine in an electron ionization source[24].

Cross sections (CSs) for the reaction of both ions as a function of the photon energy (E_{phot}) at fixed collision energy (E_{CM}) are given in **Fig. 1**, while in **Fig. 2**. CSs as a function of the collision energy are shown. In **Table 2** results obtained at a fixed E_{phot} = 11.48 eV and fixed E_{CM} =0.13 eV are summarized, by reporting the branching ratios (BRs) and the total rate constants $k_{tot}(E_{ave})$. The latter have been estimated using the expression $k_{tot}(E_{ave}) = \langle v \rangle \cdot \sigma_{tot}$, were σ_{tot} is the total reactive CS (i.e. sum over all product channels), <v> is the average relative velocity, and E_{ave} is the average energy that can be obtained from the collision energy $E_{ave} = E_{CM} + 3/2\gamma k_B T$[1] [33, 34]. The ratio between k_{tot} and the Langevin collision rate constant (k_L), also reported in **Table 2**, is a useful estimate of the overall efficiency of the reactions, which proceed at a smaller rate than the Langevin limit, namely 16% and 26% of k_L for $HCNH_2^{\bullet+}$ and $H_2CNH^{\bullet+}$ respectively.

Table 2. Total rate constants at fixed average energy $k_{tot}(E_{ave})$ and branching ratios (BRs) for the reaction of $HCNH_2^{\bullet+}$ and $H_2CNH^{\bullet+}$ with C_2H_4. Results have been obtained at fixed E_{phot} =11.48 eV and E_{CM} = 0.13±0.01 eV, corresponding to an average energy E_{ave}=0.15±0.01.

	$HCNH_2^{\bullet+}$	$H_2CNH^{\bullet+}$
$k_{tot}(E_{ave})$ [a]	$(2.0\pm0.5)\times10^{-10}$	$(3.3\pm0.9)\times10^{-10}$

[1] γ=0.508 is the ratio of the parent ion mass over the sum of the masses of charged and neutral reagents; k_B is the Boltzmann constant and T is the gas temperature in the scattering cell (~300 K in our set-up)

k_{tot} / k_L [b]	0.16	0.26
product (m/z)	**Branching ratios (BRs)**	
28	0.05 [c]	0.24 ± 0.11
30	0.43 ± 0.16	0.23 ± 0.10
42	0.010 ± 0.005	0.08 ± 0.03
56	0.51 ± 0.20	0.44 ± 0.18

[a] Total (i.e., summed over all the product channels) rate constant (in $cm^3 \cdot molecule^{-1} \cdot s^{-1}$) at the specified average collision energy E_{ave}, estimated as detailed in the text.
[b] For both isomers $k_L = 1.27 \times 10^{-9}$ $cm^3 \cdot molecule^{-1} \cdot s^{-1}$ is the Langevin rate constant, calculated using the value 4.188 $Å^3$ for the average electronic polarizability of C_2H_4
[c] Upper limit value

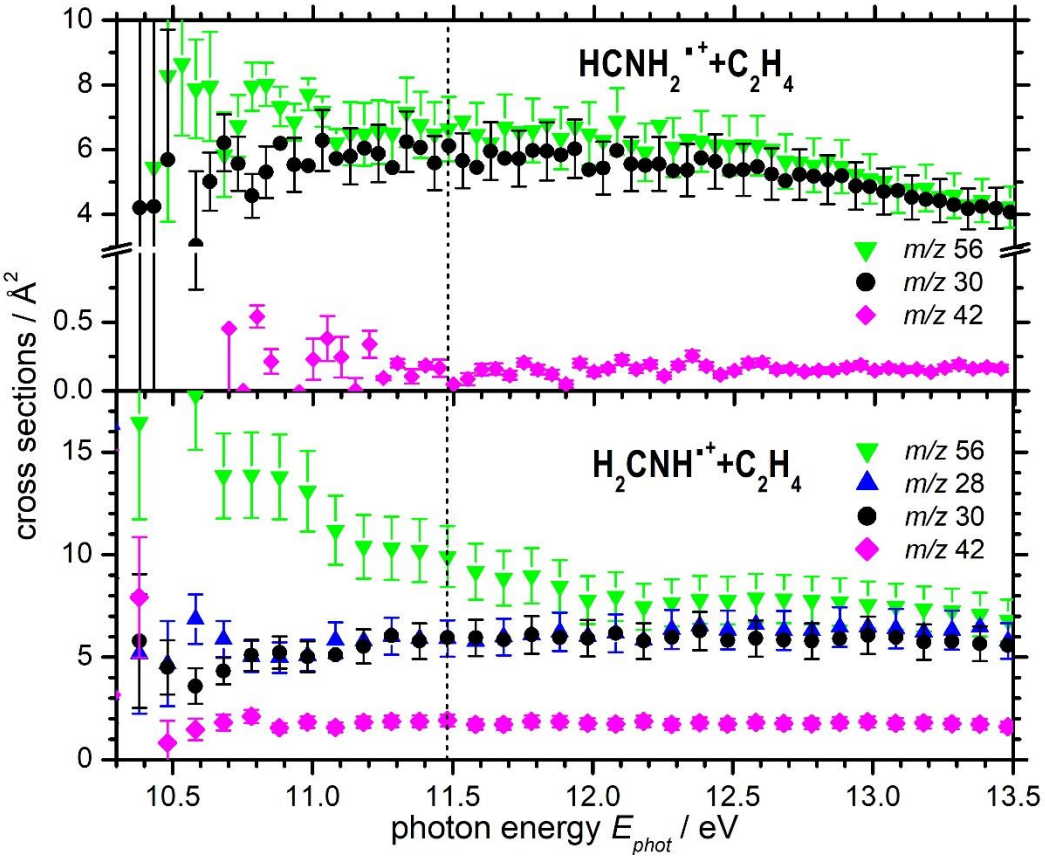

Fig. 1: Reactive cross sections as a function of E_{phot} for the reaction of $HCNH_2^{\bullet+}$ (top) and $H_2CNH^{\bullet+}$ (bottom) with C_2H_4 . Collision energies are E_{CM}=0.15 eV (top) and E_{CM}=0.13 eV (bottom). The vertical dashed lines indicate the photon energy at which data have been collected as a function of E_{CM} (see **Fig. 2**)

The *m/z* 56 product is the major one at all photon energies for both isomers. For the $HCNH_2^{\bullet+}$ isomer, this channel shows no significant dependence on E_{phot} indicating that it proceeds independently of the internal energy of the reactant ion. The decrease in CS at E_{phot} > 12.4 eV, also observed for the other major product at *m/z* 30, is an artefact due to the increasing contamination of $C_2H_5^+$ in the parent beam (see discussion in the **Supplementary Information - Part 2**), which reduces the relative amount of $HCNH_2^{\bullet+}$ ion available for reaction. The next most significant product for the $HCNH_2^{\bullet+}$ isomer is at *m/z*

30, with similar trend with E_{phot} as *m/z* 56. A minor channel at *m/z* 42 is detected and approximately constant (within uncertainty) as a function of E_{phot}.

For the $H_2CNH^{\bullet+}$ isomer, after the *m/z* 56 channel, the *m/z* 28 and 30 are the next most significant pathways, with equivalent CSs over the entire photon energy range. It is worth noting that at low photon energies the *m/z* 56 channel shows initial decrease before levelling off above 12 eV, whereas the *m/z* 30 channel undergo a slight increase over this same photon energy range. This is discussed further in **Section 5**. The minor channel at *m/z* 42 is also observed, being largely constant but notably more intense than for the other isomer.

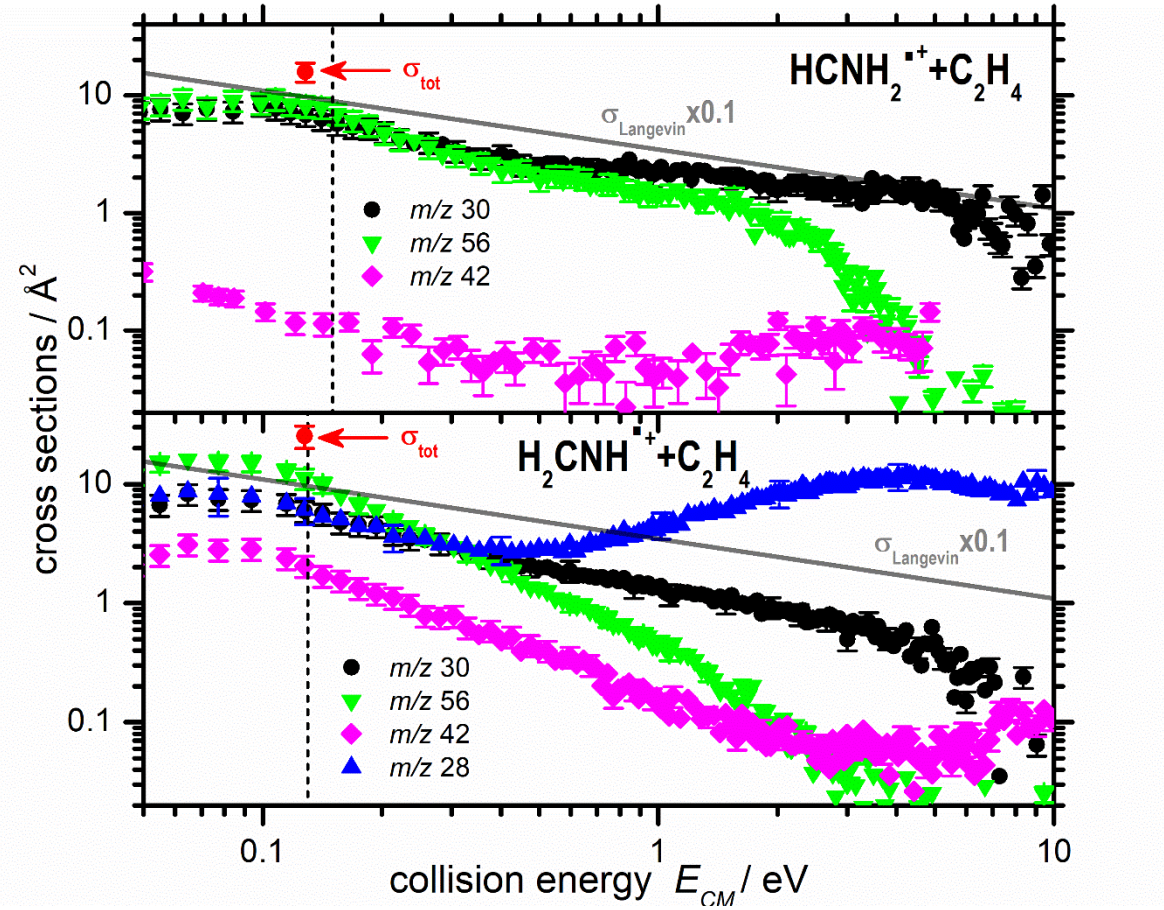

Fig. 2: Reactive cross sections as a function of the collision energy E_{cm} for the reaction of $HCNH_2^{\bullet+}$ (top) and $H_2CNH^{\bullet+}$ (bottom) with C_2H_4. The photon energy is fixed at E_{phot}=11.48 eV, with the exception of *m/z* 42 from $HCNH_2^{\bullet+}$ for which is equal to 12.48 eV. The vertical dashed lines indicate the collision energy at which data have been collected as a function of E_{phot} (see **Fig. 1**). The grey solid lines are the Langevin CSs (rescaled by a factor 0.1 to fit in the figure) that are identical for both isomers. The red points are the total reactive CSs (σ_{tot}) used to calculate the total rate constants k_{tot} reported in **Table 2**.

The trends as a function of the collision energy (**Fig. 2**) are very similar for the *m/z* 30 from both isomers, with a gradual decrease with increasing E_{CM} indicative of a barrierless exothermic process. It is worth noting that the *m/z* 30 products follow closely (at least at the

low energies) the $E^{-0.5}$ kinetic energy dependence trend represented by the Langevin capture cross sections (shown in **Fig. 2** as grey lines, rescaled by a factor 0.1 to fit in the figure). Products at *m/z* 56 from both isomers show a slightly sharper decrease with increasing collision energy, indicative of a mechanism proceeding via adduct formation. This decrease is notably sharper for the $H_2CNH^{\bullet+}$ isomer (see **Section 5** for a possible explanation).

The *m/z* 42 channel also shows a similar trend for both isomers, with a predominant low collision energy peak typical of a barrierless mechanism with a secondary rise at higher collision energies, indicating a second process involving an energy barrier. It should be noted that, while in **Fig. 2** two different E_{phot} are used for *m/z* 42 from the two isomers, the lack of photon energy dependence for this product in the explored range (see **Fig. 1**) can be used to infer that no significant change is expected when comparing data taken at different values of E_{phot} .

The *m/z* 28 product, only measured with $H_2CNH^{\bullet+}$, shows an initial decrease with increasing collision energy indicative of a barrierless process, but then displays a significant rise to a plateau. This is a strong indication of the combination of a barrierless channel with either an endothermic pathway or one having an energy barrier. A detailed discussion of the trends of all products in light of computational results is presented in **Section 5**.

4. Computational Results

In agreement with previous theoretical studies,[26,35] our calculations show that the aminocarbene ($HCNH_2^{\bullet+}$) is more stable than the methanimine radical cation ($H_2CNH^{\bullet+}$) by about 17.9 kJ·mol^{-1} and the two isomers are separated by an isomerisation barrier for 1,2-H shift of ~280 kJ·mol^{-1} (with respect to $H_2CNH^{\bullet+}$ energy). This value is substantially higher than the barrier associated to H loss from either isomer, thus making dissociation favoured over isomerization.

The two isomers are able to form both van der Waals complexes and covalently-bound adducts with ethene. In both cases, the van der Waals complex results from the approach of the ion to the neutral by the non-radical terminus, whereas the covalent adducts are formed by approach to the neutral by the radical end.

Please note that the relative enthalpies reported in the figures are given (in kJ·mol^{-1}) with respect to the sum of the energies of the separated reactants having the lowest energy (*i.e.* $HCNH_2^{\bullet+}$ plus C_2H_4). However, the reaction enthalpies of the various channels as reported in **Table 1** and in the text, are calculated with respect to the specific reactant (either $HCNH_2^{\bullet+}$ or $H_2CNH^{\bullet+}$).

$HCNH_2^{\bullet+}$ isomer (pathways are described graphically in **Fig. 3** and **4**, while reaction enthalpies are compared with literature values in **Table 1**): two different van der Waals complexes resulting from the N-terminal approach of the ion to C_2H_4 can be formed, namely **A1** and **A4**. They differ for the orientation of the H on the C atom of the ion: in **A1** the H is *Z*- to the H of the NH_2 group directed towards the π bonding system of ethene, whereas in **A4** it is *E*-. From **A1** the formation of the covalently-bound adduct **A2** proceeds via the

transition state (TS) **A1-2**. **A2** can readily eject an H via TS **A2-P** to give the *m/z* 56 product $CH_2CHCHNH_2^+$ (reaction **4a**, calculated enthalpy $\Delta H_0°$ =-112.9 kJ·mol^{-1}= -1.17 eV, see **Table 1** and **Fig. 3**). The other major product channel is the *m/z* 30 one, which can be formed in two ways. Firstly, from **A2** which undergoes an isomerization to **A3** via TS **A2-3** prior to a barrierless fragmentation into $H_2CNH_2^+$ and $C_2H_3^•$ (reaction **2**, calculated enthalpy $\Delta H_0°$ = -28 kJ·mol^{-1}= -0.29 eV, see **Table 1** and **Fig. 3**). Alternatively it can be formed via **A4**, which can transfer an H atom to give the cluster **A5** via TS **A4-5**. This species can then barrierlessly fragment to the same products.

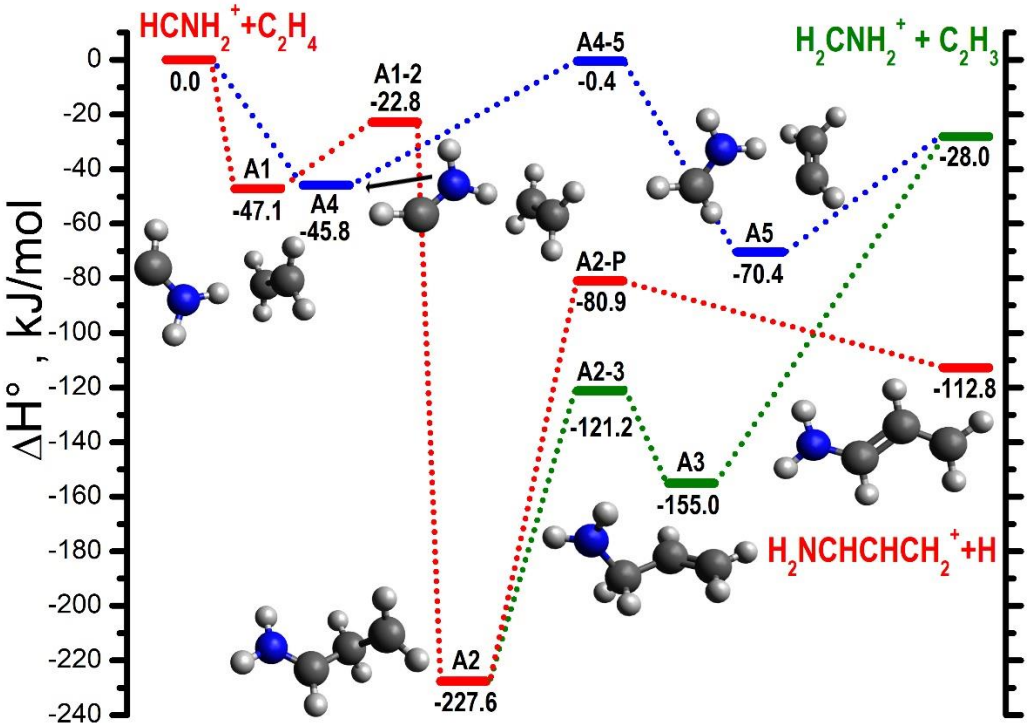

Fig. 3. ***$HCNH_2^{•+}$ plus C_2H_4***: relative enthalpies (at 0 K) and reaction pathways leading to products $H_2CNH_2^+$ plus $C_2H_3^•$ (in blue and green) and $NH_2CHCHCH_2^+$ plus $H^•$ (in red). The zero value for enthalpies (in kJ·mol^{-1}) corresponds to the separated $HCNH_2^{•+}$ plus C_2H_4 reactants. Calculations are at the MP2/cc-pVTZ//CCSD(T)/cc-pVTZ level of theory. Ball-and-stick structures refer to stable intermediates, whereas TS structures are given in the **Supplementary Information - Part 1.**

The formation of the *m/z* 42 product from $HCNH_2^{•+}$ can proceed from **A2** via TS **A2-6** to give **A6**. This can rearrange to **A7** via TS **A6-7**. **A7** can then transform, via TS **A7-8**, to **A8** which subsequently fragments barrierlessly to give protonated ketenimine ($CH_2CNH_2^+$) plus $CH_3^•$ (reaction **3**, calculated enthalpy $\Delta H_0°$ =-51.2 kJ·mol^{-1}= -0.53 eV, see **Table 1** and **Fig. 4**). Although we have not measured the E_{phot} and E_{CM} trends of the CSs for the *m/z* 28 product from this isomer as the signal was too minor to make it separatable from the parent beam, a submerged pathway for its formation is here presented. **A2** can convert into its rotamer **A9** via TS **A2-9**. **A9** can undergo a [1,4] H shift to give **A10** via TS **A9-10**. **A10** can then convert into the rotamer **A11** via TS **A10-11**. In turn, **A11** can cleave the central C-C

bond to form **A12**, a complex of $HCNH^+$ and $C_2H_5^{\bullet}$, via TS **A11-12**. This complex can barrierlessly fragment to give products (reaction **1a,** calculated enthalpy $\Delta H_0°$ = -21.7 kJ·mol^{-1}= -0.22 eV, see **Table 1** and **Fig. 4**).

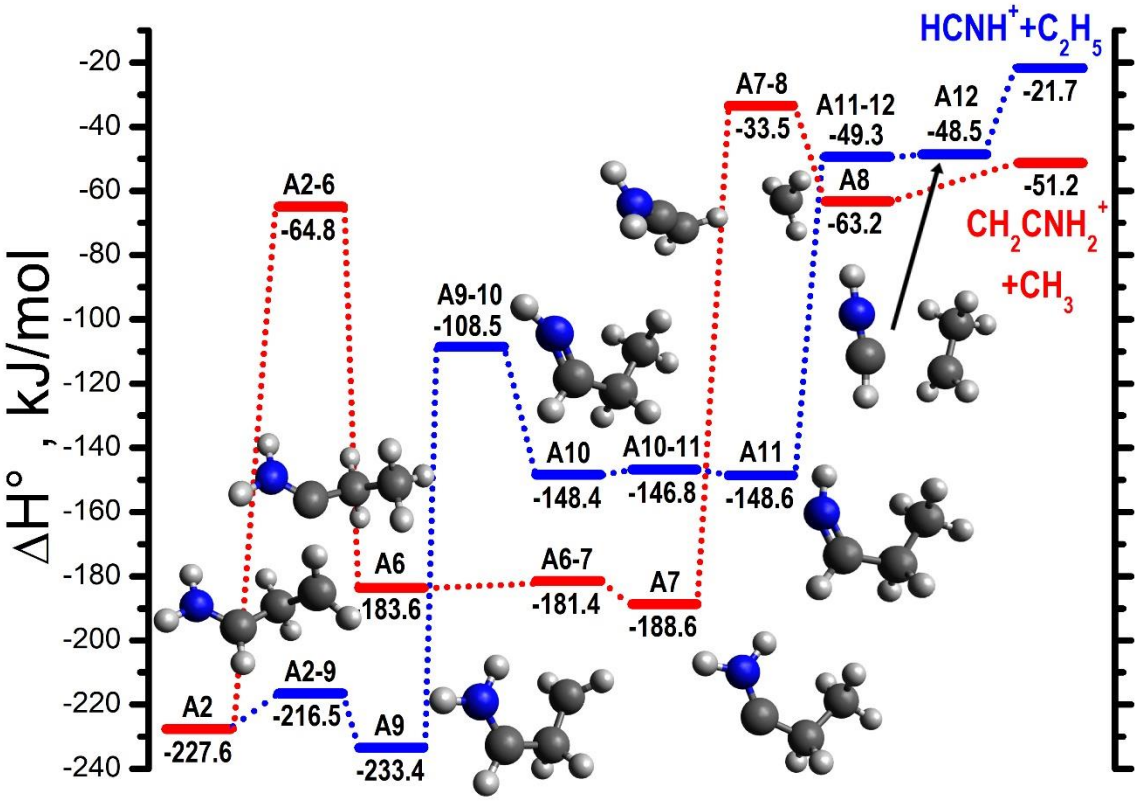

Fig. 4. ***$HCNH_2^{\bullet+}$ plus C_2H_4***: relative enthalpies (at 0 K) and reaction pathways leading to products $HCNH^+$ plus $C_2H_5^{\bullet}$ (in blue) and $CH_2CNH_2^+$ plus $CH_3^{\bullet}$ (in red). The zero value for enthalpies (in kJ·mol^{-1}) corresponds to the separated $HCNH_2^{\bullet+}$ plus C_2H_4 reactants. Calculations are at the MP2/cc-pVTZ//CCSD(T)/cc-pVTZ level of theory. Ball-and-stick structures refer to stable intermediates, whereas TS structures are given in the **Supplementary Information - Part 1.**

$H_2CNH^{\bullet+}$ isomer (pathways are described graphically in **Fig. 5** and **6**, while reaction enthalpies are compared with literature values in **Table 1**): the covalently bound adduct **B1** is formed barrierlessly. From **B1** two pathways are possible to form different isomeric products at *m/z* 56. In one case **B1** can rearrange into its rotamer **B2** via TS **B1-2**. This can then eject an H to form $CH_2NHCHCH_2^+$ via TS **B2-P** (reaction **4c**, calculated enthalpy $\Delta H_0°$ = -76.3 kJ·mol^{-1}= -0.79 eV, see **Table 1** and **Fig. 6**). An alternative pathway proceeds through **B1** cyclisation to give **B3** via TS **B1-3.** This can then eject a H to give c-$CH_2CH_2CHNH^+$ via TS **B3-P** (reaction **4b**, calculated enthalpy $\Delta H_0°$ =-69.2 kJ·mol^{-1}= -0.72 eV, see **Table 1** and **Fig. 5**).

The $H_2CNH^{\bullet+}$ isomer also has two possible mechanisms for formation of products at *m/z* 30 amu, though only one is fully submerged. This pathway proceeds via the van der Waals complex **B4** (see **Fig. 5**) and involves an H transfer from C_2H_4 to the ion to give structure

A5 (already mentioned in the reactivity of $HCNH_2^{\bullet+}$, see **Fig. 3**) via TS **B4-A5**. **A5** can barrierlessly separate to form $H_2CNH_2^+$ plus $C_2H_3^\bullet$ (reaction **2**, calculated enthalpy $\Delta H_0° = -45.9$ kJ·mol^{-1}= -0.48 eV, see **Table 1** and **Fig. 6**). The other mechanism requires the rearrangement of **B2** into **B5**, an isomerisation that is hampered by a barrier of 28 kJ·mol^{-1} above reagents going via TS **B2-5**. Subsequently, the barrierless rupture of the C-N bond in **B5** leads to products (see **Fig. 6**).

The formation of the other major product at *m/z* 28 first involves a [1,4] H shift from **B1** to give **B6** via TS **B1-6**. **B6** can then rearrange to form its rotamer **B7** via TS **B6-7**. This can then cleave the central C-N bond to give **B8**, a van der Waal complex of $HCNH^+$ and $C_2H_5^\bullet$ via TS **B7-8**. **B8** can then separate barrierlessly to give products $HCNH^+$ plus $C_2H_5^\bullet$ (reaction **1a**, calculated enthalpy $\Delta H_0° = -39.6$ kJ·mol^{-1}= -0.41 eV, see **Table 1** and **Fig. 5**).

The mechanism for formation of *m/z* 42 product proceeds from **B2** via TS **B2-9** to give **B9**. This can then transform to its rotamer **B10** via TS **B9-10** which in turn can fragment via TS **B10-P** to give $CH_2NCH_2^+$ and $CH_3^\bullet$ (reaction **3**, calculated enthalpy $\Delta H_0° = -67.1$ kJ·mol^{-1}= -0.70 eV, see **Table 1** and **Fig. 6**).

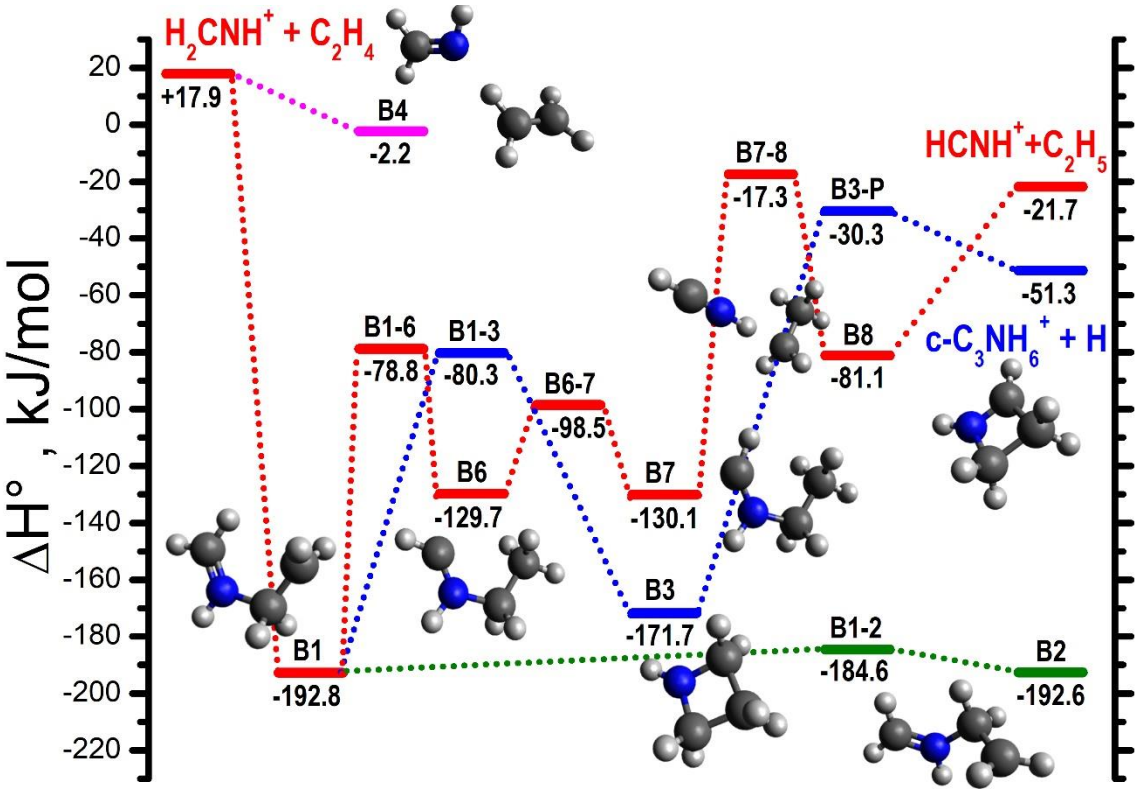

Fig. 5. ***$H_2CNH^{\bullet+}$ plus C_2H_4***: relative enthalpies (at 0 K) and reaction pathways leading to products $HCNH^+$ plus $C_2H_5^-$ (in red) and c-$CH_2CH_2CHNH^+$ plus H^- (in blue). The zero value for enthalpies (in kJ·mol^{-1}) corresponds to the separated $HCNH_2^{\bullet+}$ plus C_2H_4 reactants (same **as Fig. 3** and **4**). Calculations are at the MP2/cc-pVTZ//CCSD(T)/cc-pVTZ level of theory. Ball-and-stick structures refer to stable intermediates, whereas TS structures are given in the **Supplementary Information - Part 1.**

5. Discussion

The chemistry of $HCNH_2^{\bullet+}$ is dominated by processes involving the formation of intermediate adducts, with all three main channels proceeding at least partly in this way. However, the *m/z* 30 channel may proceed additionally via a direct H atom transfer, as discussed in the accompanying paper [16]. The *m/z* 56 channel is expected to be the major product going via an adduct pathway as this is the most exothermic channel and only involves a couple of rearrangements (from the initial van der Waals cluster **A1** to **A3**) for formation. It is therefore the most favoured channel both kinetically and thermodynamically.

For $H_2CNH^{\bullet+}$, the decrease in the *m/z* 56 product with increasing collision energy is more pronounced. This difference can be attributed to the fact that the lowest energy pathway proceeds via a cyclisation, which is likely to be sterically inhibited by increasing the collision energies, whereas this is not the case for $HCNH_2^{\bullet+}$ where the H ejection pathway proceeds via open structures. A similar explanation holds for the slight decrease in CS as the photon energy (and by extension the internal energy of the $H_2CNH^{\bullet+}$ reactant) is increased, since internal energy inhibits the cyclisation, and while there is a direct ejection pathway with submerged barriers (see **Fig. 6**), this involves higher barriers than the pathway via the cyclised adduct.

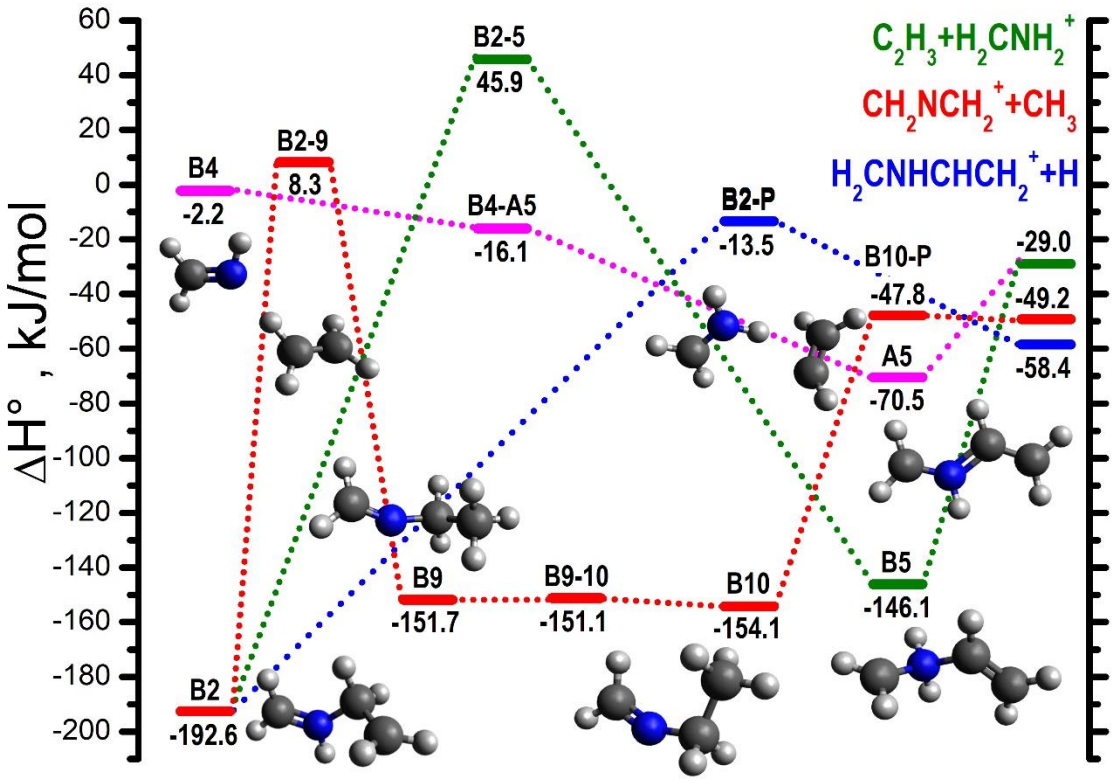

Fig. 6. ***$H_2CNH^{\bullet+}$ plus C_2H_4***: relative enthalpies (at 0 K) and reaction pathways leading to products $CH_2CNH_2^+$ plus $CH_3^{\bullet}$ (in red), $H_2CNH_2^+$ plus $C_2H_3^{\bullet}$ (in green and pink) and $CH_2NHCHCH_2^+$ plus $H^{\bullet}$ (in blue). The zero value for enthalpies (in $kJ \cdot mol^{-1}$) corresponds to the separated $HCNH_2^{\bullet+}$ plus C_2H_4 reactants (same as Figs. 3-5). Calculations are at the MP2/cc-pVTZ//CCSD(T)/cc-pVTZ level of theory. Ball-and-stick

structures refer to stable intermediates, whereas TS structures are given in the **Supplementary Information - Part 1.**

Interestingly, calculations predict different structures for the $C_3H_6N^+$ products from the two isomers. For $HCNH_2^{\bullet+}$, adduct formation proceeds through C-C bond formation, thereby leading to the most stable $C_3H_6N^+$ isomer, $CH_2CHCHNH_2^+$ (reaction **4a**, see **Table 1**). On the other hand, the radical character of the N-H terminal of the methanime radical cation leads to C-N bond formation, which favours the production of the higher energy $C_3H_6N^+$ isomers c-$CH_2CH_2CHNH^+$ and $CH_2NHCHCH_2^+$. The formation of other isomers with *m/z* 56 cannot be excluded, but a discusson of those is beyond the scope of this study.

The *m/z* 30 channel can proceed either via the covalently bound adducts or via van der Waals complexes with ethene, as well as likely exhibiting some contribution from a direct H-stripping process (see the discussion on the H atom transfer reaction with CH_4[16]). The collisional energy dependence of the CS is very similar for the two isomers, showing only a slightly more significant decrease with increasing collision energy for $H_2CNH^{\bullet+}$, likely due to the competition with the *m/z* 28 channel, which is smaller for the $HCNH_2^{\bullet+}$ isomer.

The *m/z* 28 channel shows the most significant differences between the two isomers. At low collision energies there is a fully-submerged adduct pathway to form this product with both isomers, but for $HCNH_2^{\bullet+}$ this involves significantly more rearrangement and so is kinetically more inhibited, which may explain the smaller CS (by about a factor 7) for this channel at low collision energies. At high collision energies, the $H_2CNH^{\bullet+}$ isomer shows a marked increase followed by a plateau, which is expected to correspond to the endothermic charge transfer channel (reaction **1b**, calculated enthalpy $\Delta H_0° = +53.0$ kJ·mol^{-1} = +0.55 eV), which opens up at high collision energies, thus leading to the observed double-bell effect. It should be noted that with increasing kinetic energy of the parent ion, a contribution at *m/z* 28 may also come from collision induced dissociation of the latter to give $HCNH^+$ plus H which requires at least 1.3 eV of energy for the $H_2CNH^{\bullet+}$ isomer.
The *m/z* 42 channel is minor but present for both isomers. For $HCNH_2^{\bullet+}$, there is a barrierless pathway via adduct formation, with the small CS being attributed to the fact that it requires multiple rearrangements. For $H_2CNH^{\bullet+}$, the pathway also proceeds barrierlessly via formation of a covalently bound adduct; it is thermodynamically favoured, though as it also requires a number of rearrangements it is far more kinetically inhibited than the two major channels.

Importantly, present results from the reactivity with C_2H_4 demonstrate better than reactivity with CH_4 (see our accompanying paper [16]) that the two radical cation isomers have markedly different chemistries. This is a strong evidence in support of the selectivity of our ion generation processes and of the fact that reagent ion isomerization prior to reaction is not occurring under our experimental conditions.

6. Conclusions

The reaction of the methanimine radical cation ($H_2CNH^{\bullet+}$) and its isomer aminomethylene ($HCNH_2^{\bullet+}$) with C_2H_4 is reported by measuring the dependence on both photon and collision

energies of the product CSs (in absolute values) using a guided ion beam tandem mass spectrometer with VUV dissociative ionization for ion generation. The different behaviour of products clearly show that it is possible to produce the different isomers selectively through the choice of suitable precursor molecules. It also shows that isomerisation reactions of the reactants do not occur in the present set-up. Experimental results are rationalized via reaction mechanisms proposed on the basis of ab initio calculations of the most relevant stationary points on the potential energy surfaces.

For both isomers, the channel leading to a *m/z* 56 is the primary product at low collision energies and calculations indicate that: *a)* it may proceed via H-elimination from an initially formed adduct and *b)* the structure of products is influenced by the structure of the cationic isomer. The title reactions can therefore serve as intermediate steps to form larger nitrogen-containing species in different ionic environments, including Titan's atmosphere. The channel leading to *m/z* 30 (formation of $CH_2NH_2^+$) is also prominent for both isomers, whereas the product at *m/z* 42 (elimination of a methyl radical from the adduct) is a minor feature, especially in the case of $HCNH_2^{\bullet+}$. A key difference between the reactivity of the two isomers is the product at *m/z* 28 ($HCNH^+$) which has a cross section ~ 7 times smaller in $HCNH_2^{\bullet+}$ compared to $H_2CNH^{\bullet+}$, at least at low collision energies. All observed channels show a negative dependence of the cross sections on the collision energies at low E_{CM} (smaller than 0.5 eV) which points to exoergic and barrierless processes which are feasible in cold environments like the interstellar medium and Titan's atmosphere.

Acknowledgements

We are grateful to the DESIRS beamline team for their assistance during the synchrotron measurements and to the technical staff of SOLEIL for the smooth running of the facility under projects n◦ 20180118 and 20190249. This work was supported by the European Union's Horizon 2020 research and innovation programme "Astro-Chemistry Origins" (ACO), Grant No 811312. W.G. thanks the Swedish Research Council for a project grant (grant number 2019-04332). M.P. and J.Ž. acknowledge support from the Ministry of Education, Youth and Sports of the Czech Republic (grant No. LTC20062). V.R. acknowledges funding for a PhD fellowship from the Dept. Physics, University of Trento.

Bibliography

[1] M Larsson,. W. Geppert, G. Nyman, Rep. Prog. Phys. 75 (2012) 066901
[2] R. C. Woods, C. S. Gudeman, R. L. Dickman, P. F. Goldsmith, G. R. Huguenin, W. M. Irvine, Å. Hjalmarson, L.-Å. Nyman, and H. Olofsson, Astrophys. J. 270 (1983) 583-588
[3] M. A. Cordiner, N. A. Teanby, C. A. Nixon, V. Vuitton, A. E. Thelen, S. B. Charnley, Astronomical Journal, 158 (2019) 76
[4] P.Fathi, W. D. Geppert, A.Kaiser, D.Ascenzi, Mol. Astrophys. 2, (2016) 1-11
[5] M. Polášek, E.-L. Zins, C. Alcaraz, J. Zabka, V. Krizova, L.Giacomozzi, P. Tosi, D, Ascenzi J. Phys. Chem. A 120 (2016) 5041-5052
[6] S. Brunken, F. Lipparini, A. Stoffels, P. Jusko, B. Redlich, J. Gauss, S. Schlemmer, J. Phys. Chem. A, 123 (2019) 8053-8062
[7] S. Hörst, J. Geophys. Res. Planets, 122 (2017) 432–482
[8] S. Vinatier, B. Bezard, Icarus 2007188 (2007)120–138
[9] C.A. Nixon, R.D. Lorenz, R.K. Achterberg et al. Plan. Space Sci. 155 (2018) 50–72

[10] H. Imanaka,H., M. A. Smith, ,Geophys. Res. Lett. 34 (2007) L02204.
[11] E. Vigren, J.Semaniak, M. Hamberg, V. Zhaunerchyk M. Kaminska R.D. Thomasa, M. af Ugglas, M. Larsson, W.D. Geppert, Planet. Space Sci. 60 (2012) 102
[12] J.H. Westlake, J.H. Waite, N. Carrasco, M. Richard, T. Cravens, J. Geophys. Res. A119 (2014) 5951–5963
[13] V. Vuitton, R.V. Yelle, S.J. Klippenstei, S.M. Hörst, P. Lavvas, Icarus 324 (2019) 120–197
[14] J.H. Waite, D.T. Young, T.E. Cravens, A.J. Coates, F.J. Crary, B. Magee, J. Westlake, Science 316 (2007) 870-875
[15] V. Vuitton, R.V. Yelle, M.J. McEwan, Icarus 191 (2007) 722–742.
[16] V. Richardson, C. Alcaraz, W. Geppert, J.-C. Guillemin, M. Polášek, C. Romanzin, D. Sundelin, R. Thissen, P. Tosi, J. Žabka, D. Ascenzi *Chem.Phys.Lett. (2021), accepted for publication*
[17] C. Alcaraz, C. Nicolas, R. Thissen, J. Žabka, and O. Dutuit, J. Phys. Chem. A 108 (2004) 9998–10009
[18] B. Cunha de Miranda, C. Romanzin, S. Chefdeville, V. Vuitton, J. Žabka, M. Polášek et al. , J. Phys. Chem. A 119 (2015) 6082–6098
[19] L. Nahon, N. de Oliveira, G.A. Garcia, J-F. Gil, B. Pilette, O. Marcouillé, B. Lagarde, and F. Polack, J. Synchrotron Rad. 19 (2012) 508–520
[20] E. Teloy, D. Gerlich, Chem. Phys. 4 (1974) 417 – 427
[21] M. J. Frisch, G. W. Trucks, H. B. Schlegel et al., Gaussian 09, Revision D.01, Gaussian, Inc., Wallingford CT, 2013
[22] M.J. Polce Y. Kim, C. Wesdemiotis Int. J. Mass Spectrom. Ion Proc167/168 (1997) 309-315
[23] P.C. Burgers, J.L. Holmes and J.K. Terlouw, J. Am. Chem. Soc. 106 (1984) 2762
[24] J. Chamot-Rooke, P. Mourgues, G. van der Rest, H.E. Audier, Int. J. Mass Spectrom. 226 (2003) 249–269
[25] V. G. Anicich, JPL-Publication-03-19 (2003) http://hdl.handle.net/2014/7981
[26] M.T. Nguyen, J. Rademakers, J.M.L. Martin, Chem. Phys. Lett. 221(1994) 149
[27] NIST ChemistryWebBook, NIST Standard Reference Database Number 69 (2018), Available: https://webbook.nist.gov/chemistry/ eds. P.J. Linstrom, and W.G. Mallard (Gaithersburg, MD: National Institute of Standards and Technology), 20899.
[28] J. Holmes, C. Aubry, and P. Mayer, Assigning Structures to Ions in Mass Spectrometry (2006) CRC Press, Taylor & Francis Group, Boca Raton FL (USA)
[29] J. Holmes, F.P. Lossing and P.M. Mayer, Chem. Phys. Lett. 198 (1992) 211-213
[30] A.K. Eckhardt and P.R. Schreiner, Angew. Chem. Int. Ed. 57 (2018) 5248 –5252
[31] Z. A. Harvey, J. C. Traeger Eur. J. Mass Spectrom. 10 (2004) 759–765 https://doi.org/10.1255/ejms.681
[32] G. Bouchoux, B. Gaudin, D. Leblanc, M. Yáñez and O. Mó, Int. J. Mass Spectrom. 199 (2000) 59–69. https://doi.org/10.1016/S1387-3806(00)00190-1
[33] new K. M. Ervin, P.B. Armentrout, J. Chem. Phys. 83, (1985) 166–189. doi: 10.1063/1.449799
[34] C. Nicolas, C. Alcaraz, R. Thissen, J. Žabka, and O. Dutuit, Plan. Space Sci. 50 (2002) 877–887. doi: 10.1016/S0032-0633(02)00063-6
[35] J. Zhou and H. B. Schlegel, J. Phys. Chem. A 113 (2009) 9958–9964.

Table 1. Reaction enthalpies for the reaction: $HCNH_2^{\bullet+}/H_2CNH^{\bullet+} + C_2H_4 \rightarrow$ products

Products	**Reaction**	**$\Delta H°$ with $HCNH_2^{\bullet+}$ (eV)** [a]		**$\Delta H°$ with $H_2CNH^{\bullet+}$ (eV)** [a]	
		Lit. values (298 K)	*Calc., this work (0 K)*	*Lit. values (298 K)*	*Calc., this work (0 K)*
$C_2H_5^{\bullet} + HCNH^+$	1a	-0.12±0.28 [b]	-0.22	-0.28±0.28 [b]	-0.41
$H_2CNH/ HCNH_2 + C_2H_4^{\bullet+}$	1b	+2.31±0.13 [c]	+2.30	+0.58±0.28[c]	+0.55
$C_2H_3^{\bullet} + H_2CNH_2^+$	2	-0.35±0.17[d]	-0.29	-0.52±0.17 [d]	-0.48
$CH_3^{\bullet} + C_2NH_4^+$	3	-0.46±0.20 [e] -0.49±0.20 [f]	-0.53 --	-0.63±0.20 [e] -0.66±0.20 [f]	-- -0.70
$H^{\bullet} + CH_2CHCHNH_2^+$	4a	-1.11±0.17 [g]	-1.17	-1.27±0.17 [g]	--
$H^{\bullet} + c\text{-}CH_2CH_2CHNH^+$	4b	-0.61±0.20 [g]	--	-0.77±0.20 [g]	-0.72
$H^{\bullet} + CH_2NHCHCH_2^+$	4c	-0.65±0.20 [g]	--	-0.81±0.20 [g]	-0.79

[a] All values in the Table have been evaluated using $\Delta_fH_{298}°(HCNH_2^{\bullet+})$=10.67±0.10 eV [26], $\Delta_fH_{298}°(H_2CNH^{\bullet+})$ = 10.84±0.10 eV [26] and $\Delta_fH_{298}°(C_2H_4)$ = 0.543±0.005 eV [27]

[b] Assuming the formation of $HCNH^+$ ($\Delta_fH_{298}°$ = 9.87±0.15 eV [28]) plus the ethyl radical C_2H_5 ($\Delta_fH_{298}°$= 1.23±0.02 eV[28])

[c] Assuming the formation of neutral methanimine ($\Delta_fH_{298}°$ = 0.91±0.17 eV[29]) or aminomethylene ($\Delta_fH_{298}°$ = 2.47±0.02 eV from calculations [30]) plus the $C_2H_4^{\bullet+}$ radical cation ($\Delta_fH_{298}°$ = 11.057±0.006 eV [27])

[d] Assuming the formation of the vinyl radical (C_2H_3) with $\Delta_fH_{298}°$ = 3.10±0.05 eV[27] and aminomethylium ion $H_2CNH_2^+$ with $\Delta_fH_{298}°$ = 7.77±0.01 eV[31]. This pathway is also predicted by our calculations to lead to the product ion with *m/z* 30

[e] Assuming the formation of protonated ketenimine $CH_2CNH_2^+$ ($\Delta_fH_{298}°$ = 9.24±0.09 eV [28]), as predicted to occur, by present calculations, from the $HCNH_2^{\bullet+}$ isomer (see **Sec. 4**).

[f] Assuming the formation of the $CH_2NCH_2^+$ isomer ($\Delta_fH_{298}°$ = 9.21±0.09 eV [28]), as predicted to occur, by present calculations, from the $H_2CNH^{\bullet+}$ isomer (see **Sec. 4**).

[g] Assuming the formation of various $C_3H_6N^+$ isomers, namely $CH_2CHCHNH_2^+$ with $\Delta_fH_{298}°$ = 7.85±0.06 eV **[32]**, $CH_2NHCHCH_2^+$ with $\Delta_fH°$ = 8.31±0.09 eV[28] and the $c\text{-}CH_2CH_2CHNH^+$ isomer with $\Delta_fH°$ = 8.35±0.09 eV [28]. For the latter two structures the $\Delta_fH°$ are obtained from a combination of experimental values and calculated relative energies at the G2 level of theory as detailed in [28].

Figure 1

Click here to access/download;Figure;Fig1.tif

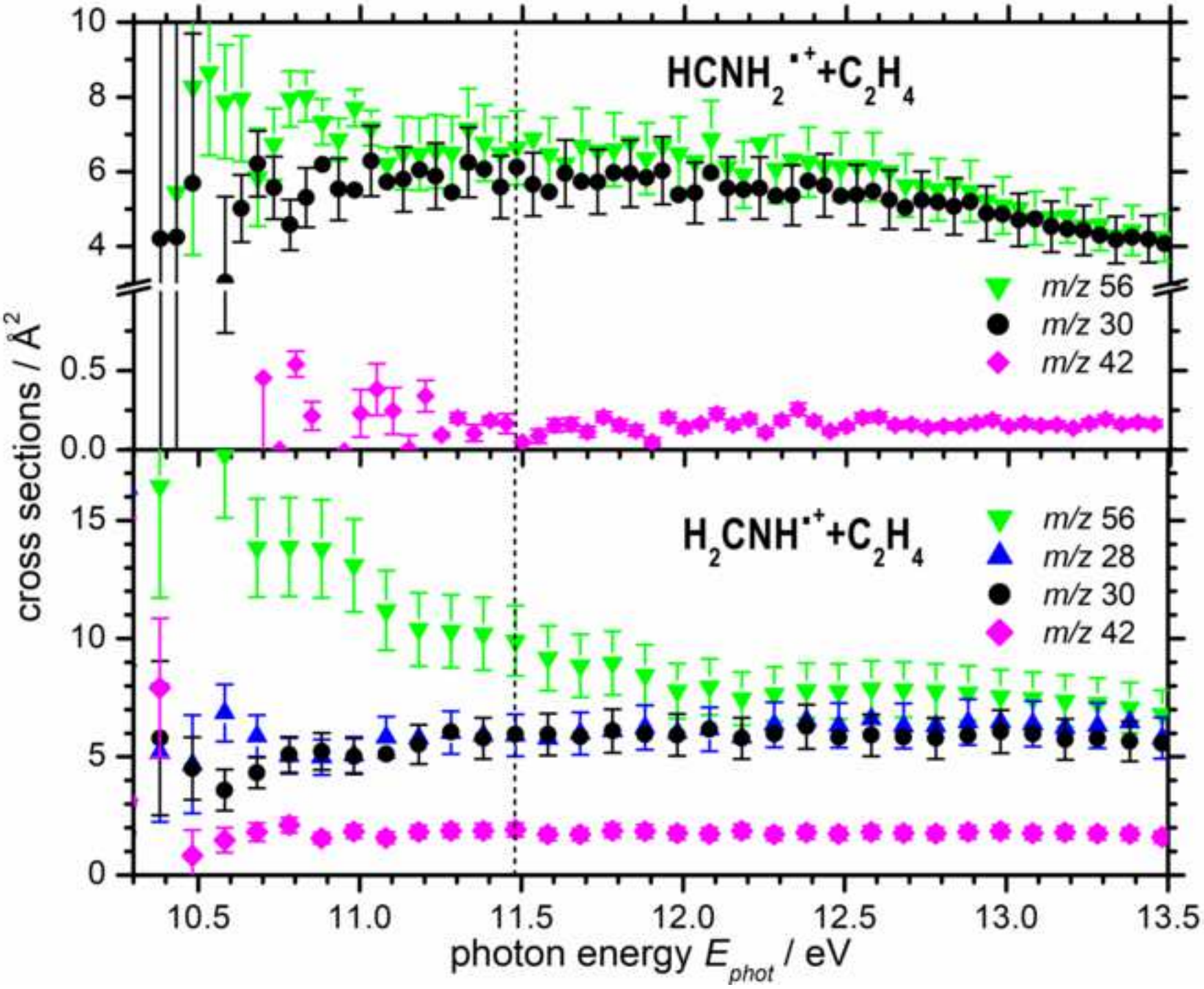

Figure 2

Click here to access/download;Figure;Fig2 rev.tif

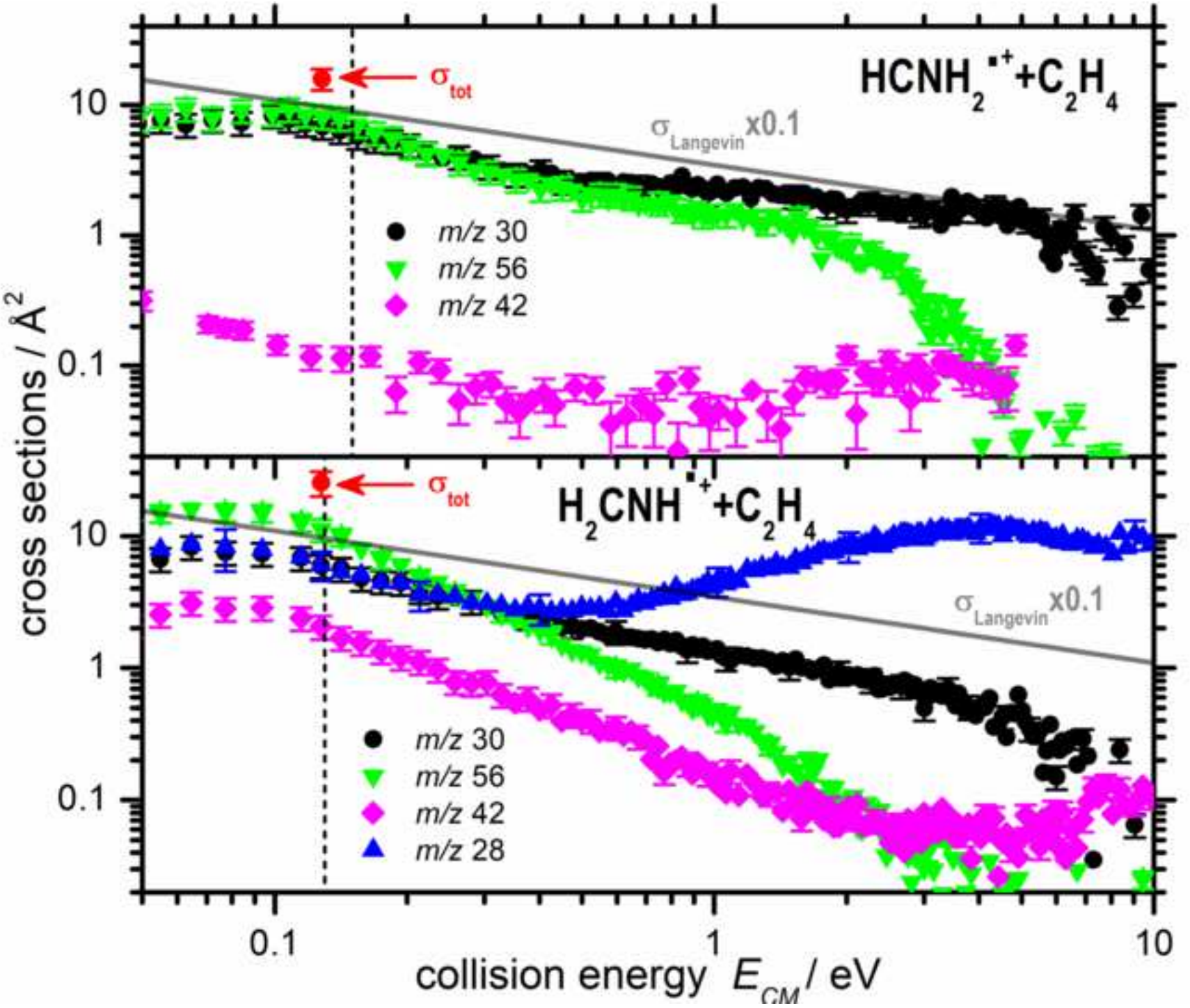

Figure 3

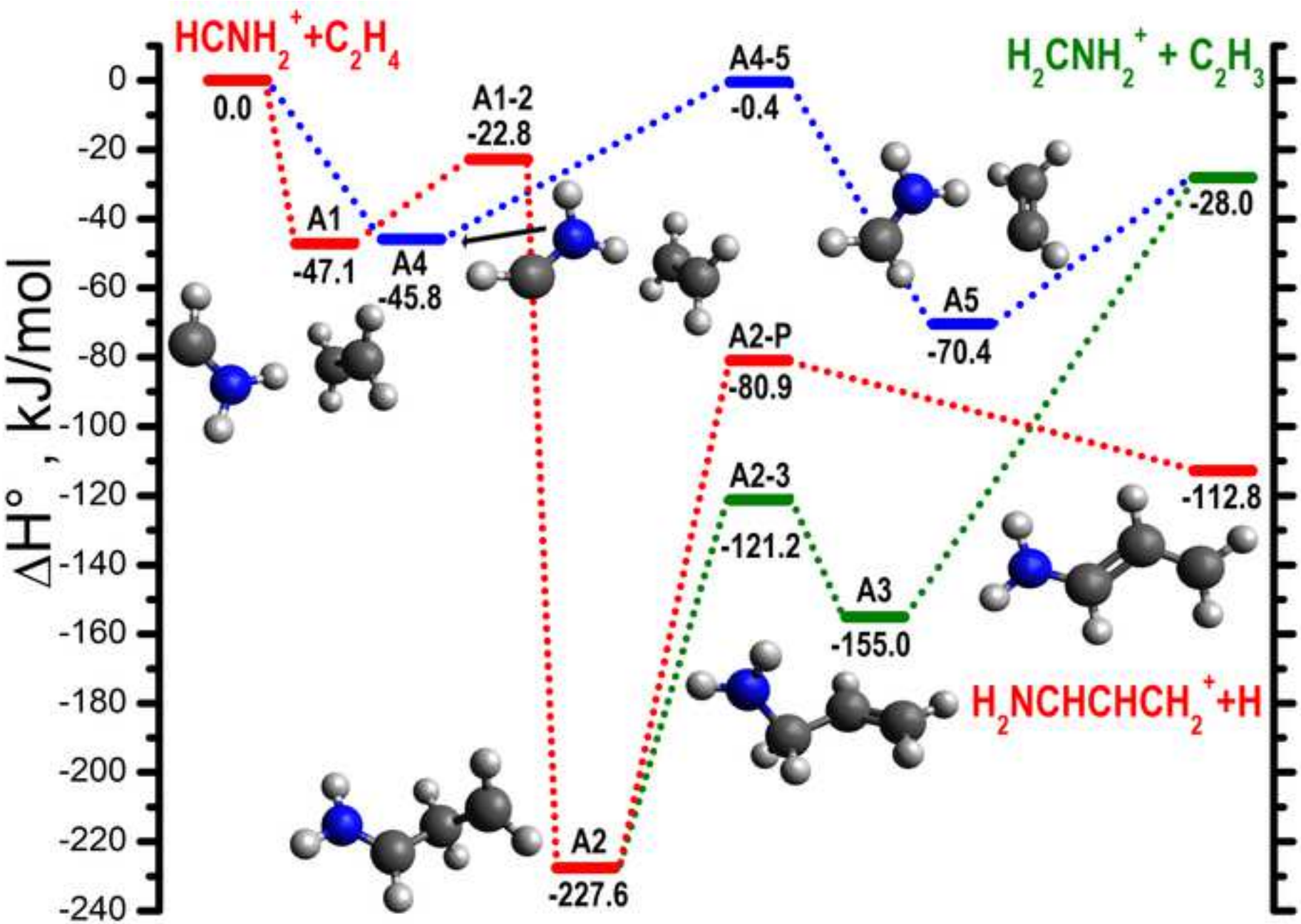

Figure 4

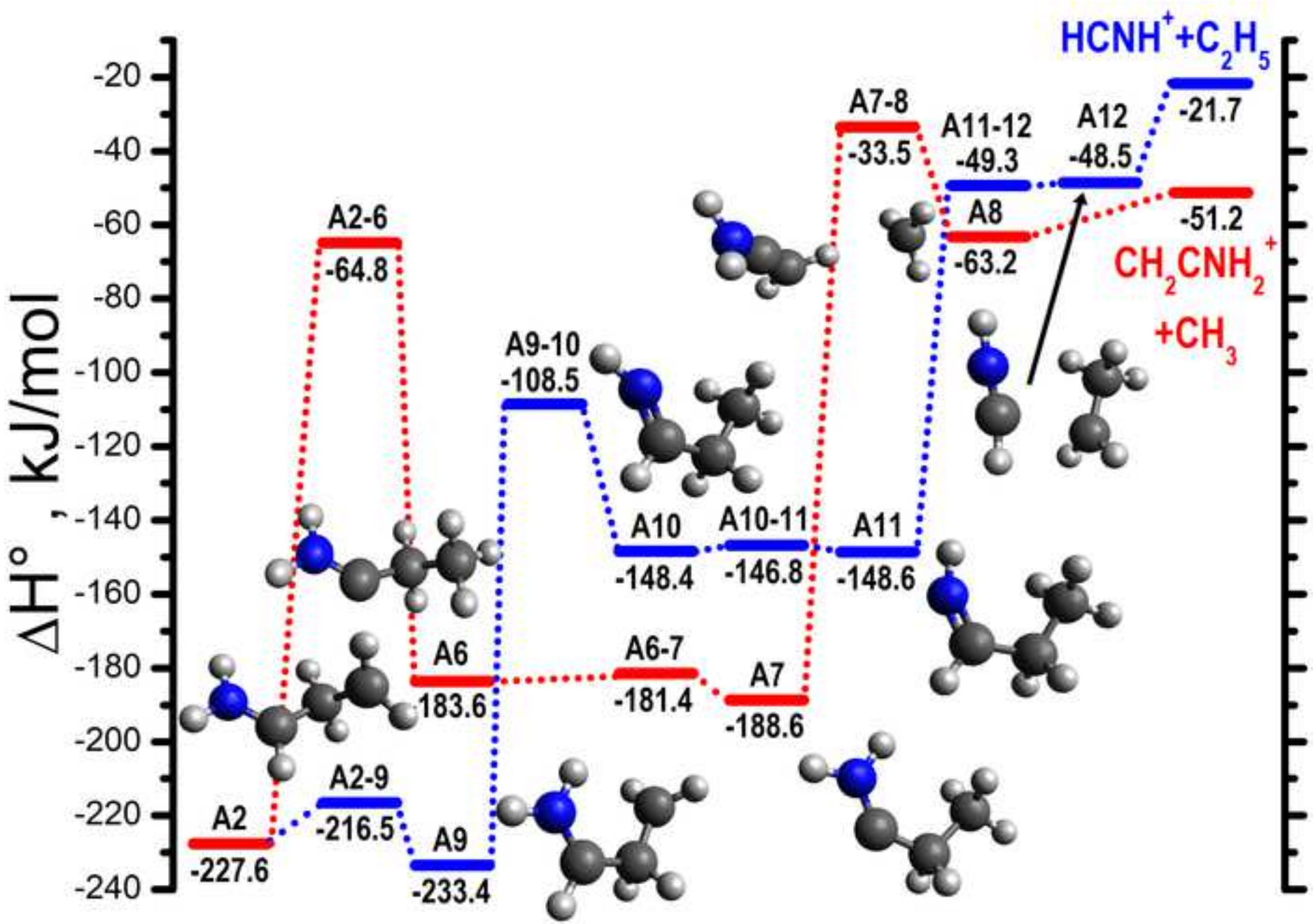

Figure 5

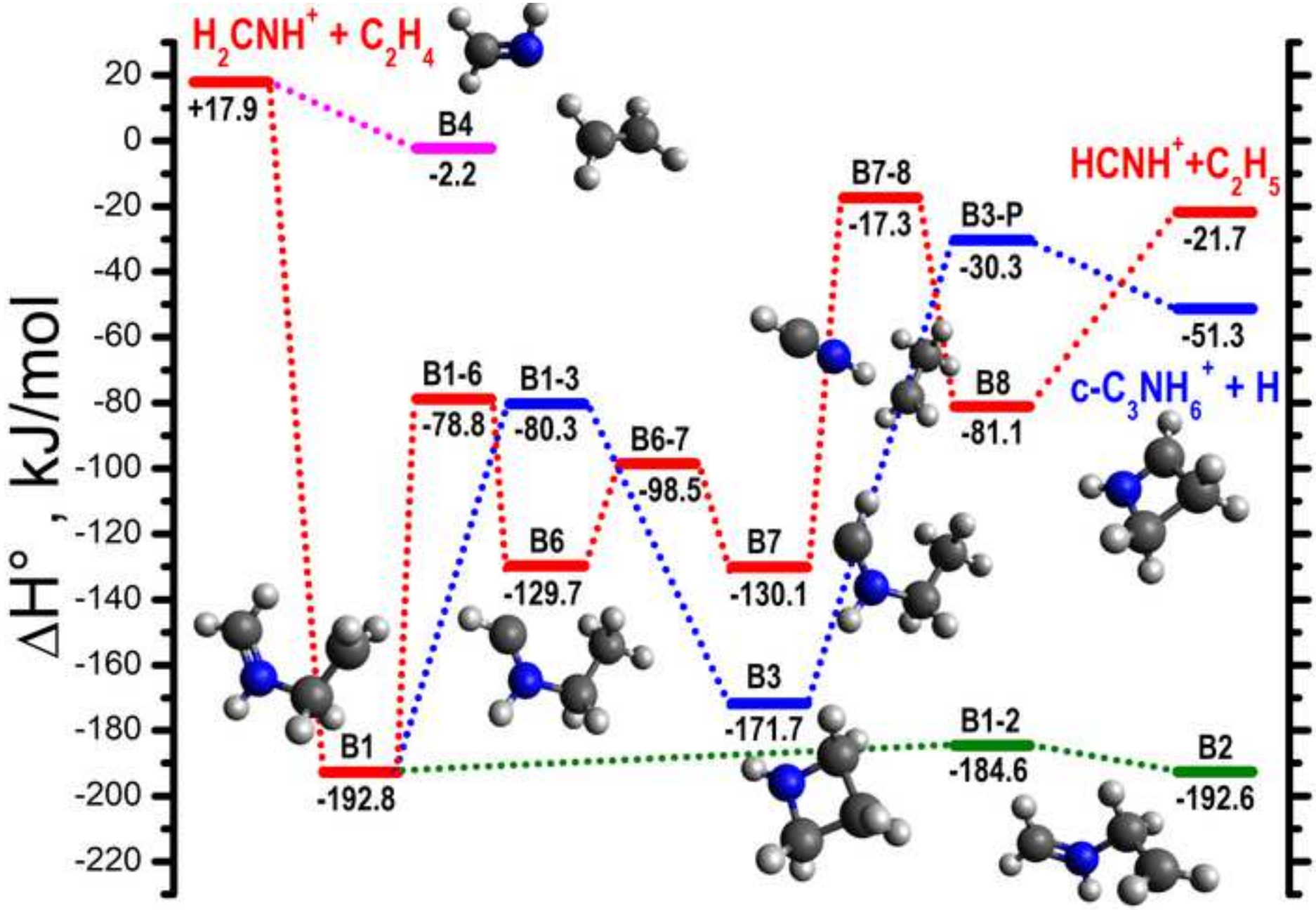

Figure 6

Click here to access/download;Figure;Fig6 rev.jpg

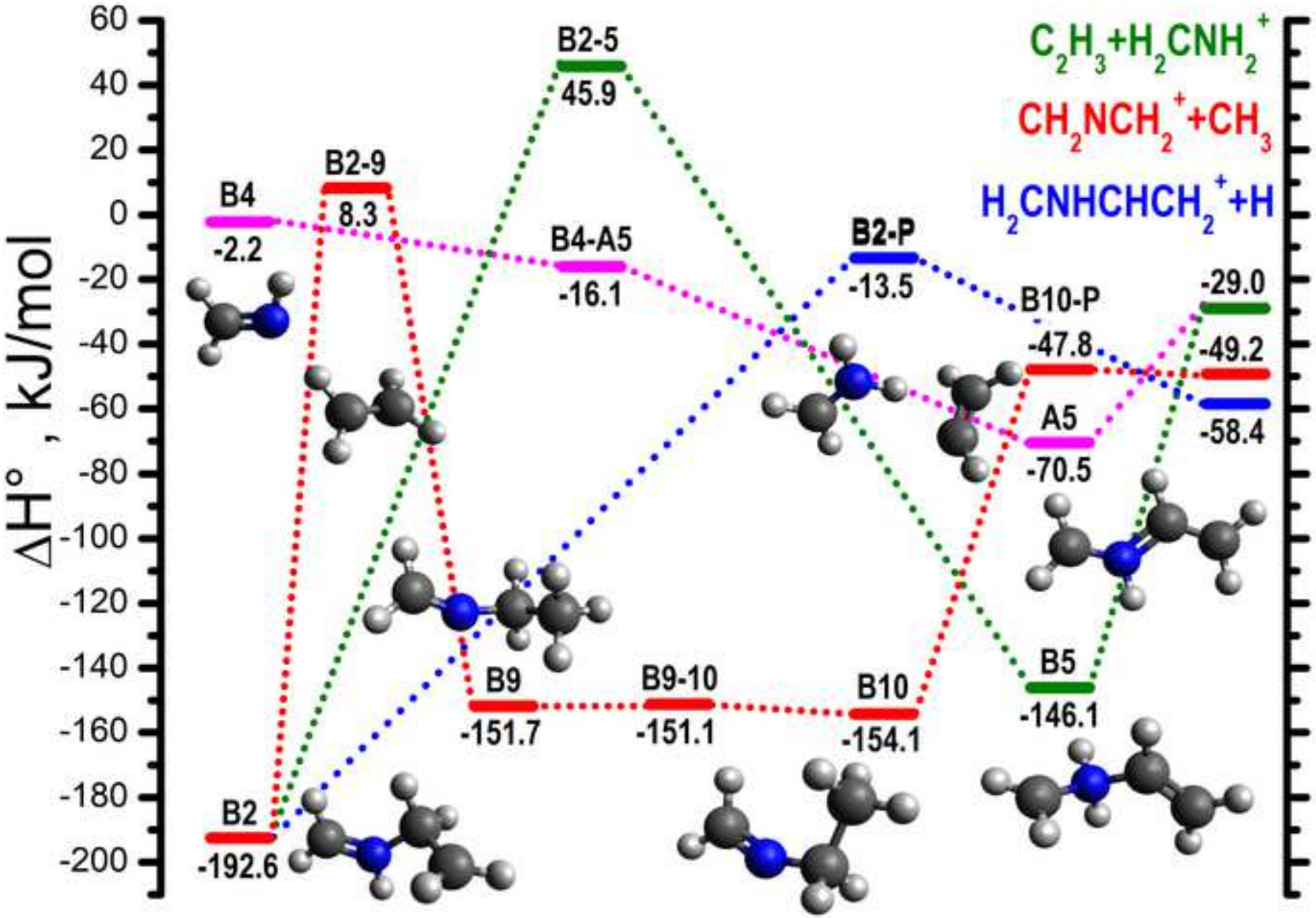

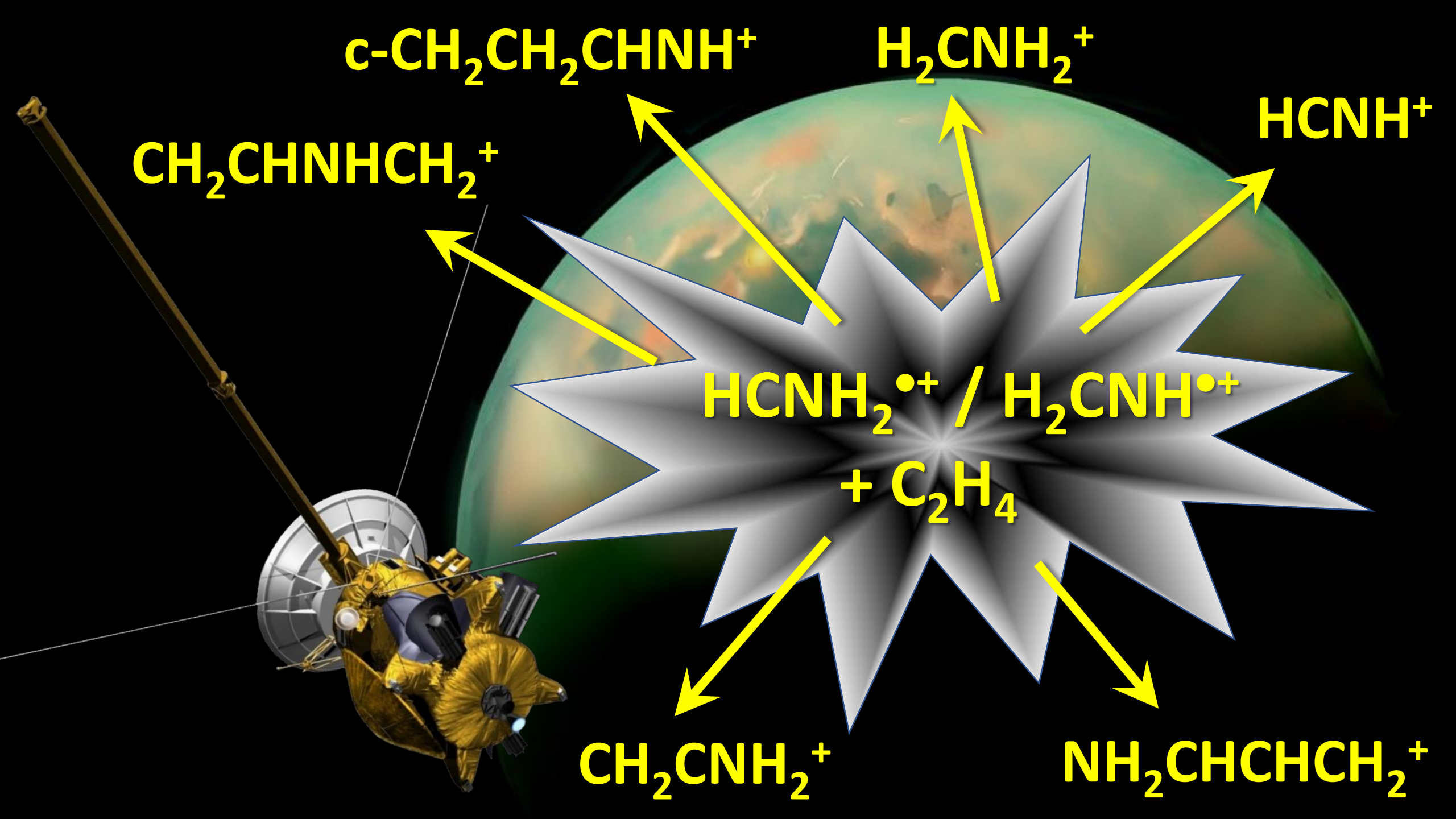
c-CH2CH2CHNH+
H2CNH2+
HCNH+
CH2CHNHCH2+
HCNH2•+ / H2CNH•+
+ C2H4
CH2CNH2+
NH2CHCHCH2+